General formulation of interactions and energy loss of particles in plasmas: Quantum-wave-packet model versus a semiclassical approach

C. D. Archubi [*] and N. R. Arista [†]

Instituto de Astronomía y Física del Espacio, Universidad de Buenos Aires, Consejo Nacional de Investigaciones Científicas y Técnicas, Ciudad Universitaria, 1428 Buenos Aires, Argentina

and Centro Atómico Bariloche and Instituto Balseiro, Comisión Nacional de Energía Atómica, 8400 S. C. de Bariloche, Argentina

(Received 29 October 2021; accepted 25 February 2022; published 14 March 2022)

In this work we present a general quantum-mechanical and statistical formulation of the process of interactions of external test particles with plasmas, considering the calculation of the energy-loss coefficients, including energy losses, mean-free paths, and straggling, and describing in detail the differences between protons, positrons, and electrons. Two relevant aspects contained in this formulation are studied: the competing action of loss and gain processes in the interaction with the plasma, and the role of thermal fluctuations in those interactions. We propose two different approaches to evaluate processes of electronic interactions in plasmas. To formulate the first approach we introduce modifications to the quantum-wave-packet dielectric method, which provides a reliable description over wide ranges of plasma densities and temperatures as compared with full quantum-mechanical dielectric theory. The second approach is a semiclassical dielectric method. It consists of including statistical quantum distributions and restrictions in the energy-loss expression, combined with the classical dielectric function for hot plasmas obtained from the linearized Vlasov-Poisson equation. We compare the results from both methods on an extensive range of parameters that include low, intermediate, and high energies, with densities and temperatures going from normal laboratory conditions to very high values, such as those of interest for studies on inertial fusion, Tokamak plasmas, and astrophysical media. We give also special consideration to the case of electrons, where the restrictions imposed by the identity with plasma electrons produce important effects.

DOI: 10.1103/PhysRevA.105.032806

I. INTRODUCTION

The question of interaction of ionized particles with plasmas is at the heart of the most relevant processes of interest in current research on magnetically and inertially confined fusion (MCF and ICF, respectively) and in astrophysical studies such as those related to particle and energy transport in stellar interiors. The long-standing goal of producing energy in fusion reactors is one of those relevant cases where particle-plasma interactions as well as particle-wall interactions play a central role. This goal has proven elusive, largely due to a number of scientific and technically unsolved problems. Some of the main environments where particle-plasma interactions are of central interest, including laboratory and astrophysical plasmas, have been outlined in previous publications and in references contained therein [1–8]. Regarding the question of energy-loss processes, much work has been done over the years in relation with stopping power of ion beams [9–23], which is a subject of great interest in relation with plasma heating by injection of neutral beams in Tokamak devices [2,24–26], with the use of ion beams in ICF experiments [27–29], and with the behavior of alpha particles produced by nuclear fusions [30,31], to name the most relevant cases, but much less has been done in relation to lighter particles.

Although a description of the statistical and quantum effects of thermal excitations was presented early [11], with particular consideration of the cases of protons and alpha particles, and general features were illustrated in advanced plasma literature [32,33], a complete study of the statistical effects on the interactions and energy-loss moments (ELMs) of heavy and light particles (such as electrons or positrons) is still a pending and wide open area of fundamental interest. In particular, to our knowledge, there are no calculations of ELMs for electrons in plasmas taking into account in a full way the restrictions corresponding to identical particles [34–37], as there are for solid targets [38–41]. Hence, the purpose of this work is to present a detailed study of this problem, showing the significant differences arising for all those particles.

To this end, we will first formulate a set of integral expressions required for a complete study of the statistical effects of thermal equilibrium on the energy exchange between external charged particles and the electronic excitations of the plasma. We will illustrate these effects on the three most relevant energy-loss moments: stopping power, energy straggling, and inverse mean-free path, showing the distinct characteristics that arise for the cases of heavy (such as protons, alpha particles, or heavier ions) and light particles (electrons and positrons).

[*] archubi@iafe.uba.ar
[†] arista@cab.cnea.ar

 ©2022 American Physical Society

To cover a wide range of plasma environments we show representative sets of results for plasmas of interest in ICF and magnetic-fusion experiments, on one side, and for the conditions in typical stellar interiors, such as the sun, on the other.

Moreover, we will extend this study by considering three models of dielectric functions: the well-known classical model widely used in the plasma literature [42–44], the more general quantum dielectric function for plasmas of arbitrary degeneracy [45,46], and the more recently proposed extended-wave-packet model [47] based on Gaussian wave functions within a quantum formulation [48–50].

This work is organized as follows: Section II shows a general formulation for particle-plasma interactions underlying statistical quantum effects derived from thermal induced excitations and recoil corrections. Sections III and IV describes the treatment for the two kind of excitations: individual and collective. Section V shows the calculations for heavy ions (based on the case of protons) and light projectiles: positrons and electrons. Section VI shows the results for the different projectiles calculated for three special kind of targets: plasmas with solid-state densities, fusion plasmas, and the sun's core. Finally, Sec. VII gives the summary and conclusions. Additional information on the dielectric formalism and differences between polarization and fluctuation contributions in the energy-loss moments is developed in two Appendices.

II. FORMULATION: PARTICLE-PLASMA INTERACTIONS AT FINITE TEMPERATURES

A comprehensive quantum-mechanical formulation of the interactions between an external particle with charge Ze and a plasma with temperature T, whose properties are described in terms of its dielectric function $\varepsilon(k,\omega)$, can be made starting from the interaction probability $W(\overrightarrow{q},\omega)$ given by [7,11]

$$W(\overrightarrow{q},\omega)=\frac{8\pi(Ze)^2}{\hbar q^2}N(\omega)\mathrm{Im}\left[\frac{-1}{\varepsilon(q,\omega)}\right]. \tag{1}$$

$W(\overrightarrow{q},\omega)$ represents the inelastic-scattering probability per unit time in an elementary interaction process with momentum transfer $\hbar\overrightarrow{q}=\overrightarrow{p'}-\overrightarrow{p}$ and energy transfer $\hbar\omega=E_{p'}-E_p$, where $\overrightarrow{p}$ and $\overrightarrow{p'}$ are the momenta of the particle before and after the interaction, and E_p and $E_{p'}$ are the corresponding energies, respectively. Here, in contrast to the case of zero temperature, both positive and negative frequency values are possible. Processes with $\omega<0$ correspond to *energy loss processes* by the particle ($E_{p'}<E_p$), while those with $\omega>0$ correspond to *gain processes.* (Here loss and gain processes are defined with respect to the external particle, being complementary to the corresponding gain and loss processes by the plasma.)

In this equation the factor $N(\omega)$ is the Bose function

$$N(\omega)=\frac{1}{e^{\hbar\omega/k_BT}-1} \tag{2}$$

(where k_B is Boltzmann's constant), which represents the thermal distribution of excitations in the plasma. The presence of this factor opens new perspectives concerning stimulated or induced processes, including loss and gain effects in energy exchange, not present in most of the treatments of plasma stopping power. This makes an important difference with respect to the formulation by most of the authors and will be particularly important in treating the interaction of light particles (like positrons or electrons) with classical or quantum plasmas, as well as to calculate energy-loss moments of heavy particles.

Finally the term $\mathrm{Im}[-1/\varepsilon(k,\omega)]$, called the energy-loss function (ELF), carries the information on the screening and absorption properties of the plasma (equivalent to the oscillator strength distribution in the treatment of atomic excitations).

Following this, we calculate the mean values of the n-order moments of the energy loss $\hbar\omega$ given by

$$\frac{d\overline{E}^{(n)}}{dt}=\int\frac{d^3p'}{(2\pi\hbar)^3}(\hbar\omega)^nW(\overrightarrow{q},\omega), \tag{3}$$

and we define the *energy-loss moments* $Q^{(n)}$ (ELMs) as

$$Q^{(n)}=\frac{1}{v}\frac{d\overline{E}^{(n)}}{dt}=\frac{(Ze)^2}{\hbar v\pi^2}\int\frac{d^3q}{q^2}(\hbar\omega)^nN(\omega)\mathrm{Im}\left[\frac{-1}{\varepsilon(q,\omega)}\right]. \tag{4}$$

To perform the integrations appropriately we consider the relation between the energy and momentum transfers $\hbar\omega$ and $\hbar\overrightarrow{q}$; namely,

$$\hbar\omega=E_{p'}-E_p=\frac{1}{2m_p}[(\overrightarrow{p}+\hbar\overrightarrow{q})^2-p^2], \tag{5}$$

which yields

$$\omega=\overrightarrow{q}\cdot\overrightarrow{v}+\frac{\hbar q^2}{2m_p}, \tag{6}$$

where m_p is the incident-particle mass and $\overrightarrow{v}=\overrightarrow{p}/m_p$ is its velocity before the interaction.

Hence, the possible values of ω lie within the interval $\omega_{\min}(q,v)<\omega<\omega_{\max}(q,v)$, with

$$\omega_{\min}(q,v)=-qv+\gamma q^2, \tag{7}$$

and

$$\omega_{\max}(q,v)=qv+\gamma q^2, \tag{8}$$

where $\gamma=\hbar/2m_p$, and m_p is the projectile mass.

To reduce the integrals in Eq. (4) we separate the angular part $d\Omega_q$, $d^3q=q^2dqd\Omega_q$, where $d\Omega_q=2\pi d(\cos\theta)=2\pi dx$, (with $x=\cos\theta$), and transform the integral in x into an integral over $\omega=qvx+\hbar q^2/2m_p$, finally obtaining

$$Q^{(n)}=\frac{2}{\hbar\pi}\left(\frac{Ze}{v}\right)^2\int_0^\infty\frac{dq}{q}\int_{\omega_{\min}(q,v)}^{\omega_{\max}(q,v)}(\hbar\omega)^nN(\omega)\times\mathrm{Im}\left[\frac{-1}{\varepsilon(q,\omega)}\right]d\omega. \tag{9}$$

From this general result we consider in detail the most relevant values of ELM corresponding to $n=0$, 1, and 2, namely,

(a) Inverse mean-free path (IMFP):

$$\frac{1}{\Lambda} = Q^{(0)} = \frac{2}{\hbar\pi}\left(\frac{Ze}{v}\right)^2 \int_0^\infty \frac{dq}{q} \int_{\omega_{\min}(q,v)}^{\omega_{\max}(q,v)} N(\omega) \times \mathrm{Im}\left[\frac{-1}{\varepsilon(q,\omega)}\right] d\omega. \tag{10}$$

(b) Stopping power:

$$S = -Q^{(1)} = -\frac{2}{\pi}\left(\frac{Ze}{v}\right)^2 \int_0^\infty \frac{dq}{q} \int_{\omega_{\min}(q,v)}^{\omega_{\max}(q,v)} \omega N(\omega) \times \mathrm{Im}\left[\frac{-1}{\varepsilon(q,\omega)}\right] d\omega. \tag{11}$$

(c) Energy straggling:

$$\Omega^2 = Q^{(2)} = \frac{2\hbar}{\pi}\left(\frac{Ze}{v}\right)^2 \int_0^\infty \frac{dq}{q} \int_{\omega_{\min}(q,v)}^{\omega_{\max}(q,v)} \omega^2 N(\omega) \times \mathrm{Im}\left[\frac{-1}{\varepsilon(q,\omega)}\right] d\omega. \tag{12}$$

The minus sign in the stopping power expression agrees with the usual definition $S = -dE/dx$.

In these expressions the statistical factor $N(\omega)$ plays a most important role in changing the balance between energy-loss and -gain processes. It has two asymptotic limits: $N(\omega) \to 0$ when ω/k_BT is a large positive number, and $N(\omega) \to -1$ when ω/k_BT has a large negative value. Moreover, it has the property $N(\omega) + N(-\omega) = -1$.

One way to analyze the relevance of the thermal excitations represented by the factor $N(\omega)$ in these equations is to compare with the particular case of $T = 0$. In this case the factor $N(\omega)$ takes the form

$$N_0(\omega) = \begin{cases} 0, & \omega > 0 \\ -1, & \omega < 0. \end{cases} \tag{13}$$

We then introduce the following definition: The processes corresponding to $N(\omega)$ different from $N_0(\omega)$ will be referred to as *assisted*, or "*N*"*-processes*. We will also define as *direct* or 0*-order* processes those obtained by the replacement $N(\omega) \to N_0(\omega)$; this limiting case will be useful to evaluate the influence of *N*-processes in the calculations of the various energy-loss moments.

An alternative terminology used in some plasma physics books [32,33] refers to *polarization* and *fluctuation* terms in the energy loss. However, we think that the present terminology fits better with the quantum-mechanical framework considered here. The equivalence between these alternative terms is considered in Appendix B.

Once these definitions have been set we can write formal expressions for the 0-order and *N*-order processes. Thus, from Eqs. (9) and (13) we obtain the expression for the 0-order terms as an integral restricted to the $\omega < 0$ zone, with $N_0(\omega) = -1$; namely,

$$Q^{(n)}\big|_0 = -\frac{2}{\hbar\pi}\left(\frac{Ze}{v}\right)^2 \int_0^\infty \frac{dq}{q} \int_{\omega<0} (\hbar\omega)^n \mathrm{Im}\left[\frac{-1}{\varepsilon(q,\omega)}\right] d\omega, \tag{14}$$

and the difference between Eqs. (9) and (14) yields the contribution of *N*-order processes, consisting of two integral expressions for $\omega < 0$ and $\omega > 0$, namely $Q^{(n)}|_N = Q^{(n)}|_N^{(\omega<0)} + Q^{(n)}|_N^{(\omega>0)}$, where

$$Q^{(n)}\big|_N^{(\omega<0)} = \frac{2}{\hbar\pi}\left(\frac{Ze}{v}\right)^2 \int_0^\infty \frac{dq}{q} \int_{\omega<0} (\hbar\omega)^n [N(\omega)+1] \times \mathrm{Im}\left[\frac{-1}{\varepsilon(q,\omega)}\right] d\omega, \tag{15}$$

and

$$Q^{(n)}\big|_N^{(\omega>0)} = \frac{2}{\hbar\pi}\left(\frac{Ze}{v}\right)^2 \int_0^\infty \frac{dq}{q} \int_{\omega>0} (\hbar\omega)^n N(\omega) \times \mathrm{Im}\left[\frac{-1}{\varepsilon(q,\omega)}\right] d\omega. \tag{16}$$

The expression for the direct term, Eq. (14), agrees with the standard formula normally used to calculate the energy-loss moments of protons or other heavy particles [51,52]. It does not contain any influence of the thermally activated excitations in the plasma [other than the effects built in $\varepsilon(q,\omega)$]. As discussed in Appendix B, this term is equivalent to the *polarization* term mentioned before.

By contrast, the expressions for the induced terms, Eqs. (15) and (16), represent the influence of thermal excitations on the interactions of the test particle with plasma electrons.

As is obvious from these definitions, an interesting analogy can be traced between these processes and the well-known spontaneous and stimulated photon processes in the quantum theory of radiation.

In the next sections three different approaches will be considered: (a) the quantum dielectric function based on the exact Fermi-Dirac distribution function, covering all possible cases of plasma degeneracy (i.e., all values of the parameter k_BT/E_F, where E_F is the Fermi energy) using the formulation of Ref. [46], and to be referred to here as AB theory; (b) a quantum formulation of the dielectric function using Gaussian distribution functions, based on the so-called wave-packet model developed by Kaneko [48–50], adapted in Ref. [47] for plasmas, and referred to as the plasma wave-packet model (PWPM); (c) the classical dielectric function widely used in the plasma literature [42–44], to be referred to as the semiclassical model (SCLM). This will allow us to make comparisons and show differences between the quantum and the semiclassical approaches.

The characteristics of these alternative dielectric function are summarized in Appendix A.

III. COLLECTIVE AND INDIVIDUAL EXCITATIONS

The previous integrals for the dielectric function receive contributions from two well-know type of excitations in the plasma: collective (or plasmon) and individual excitations [51–53]. The first type of excitation is characterized by a very narrow peak in the ELF, which appears for low-q values (corresponding to long-range organized motion of plasma electrons). As shown in Ref. [17] these plasma resonances dominate the energy absorption in the plasma for q values in the range $0 < q < q_c$, where the value of q_c is of the order the

Debye screening constant, $k_D = (4\pi ne^2/k_BT)^{1/2}$, and where n is the electron density.

It is of interest to provide here a well-defined criterion to separate the regions of collective and individual excitations and to obtain a value of the intermediate wave vector q_c that could be used for a wide range of plasma conditions.

The Debye constant is a characteristic value for the screening of external charges in a classical plasma. In the more general case of plasmas of arbitrary degeneracy the screening effects can be appropriately described by a screening constant k_s given by [46]

$$k_s^2 = \tfrac{1}{2}k_{TF}^2\theta^{1/2}F_{-1/2}(\eta), \tag{17}$$

where $F_{-1/2}(\eta)$ is a Fermi integral of order $-1/2$ and $k_{TF} = \sqrt{3}\omega_P/v_F$ is the Thomas-Fermi screening constant, in terms of the plasma frequency ω_P and Fermi velocity v_F.

As shown in Ref. [46], using a simple but very good approximation for the function $F_{-1/2}(\eta)$, the following interpolation formula was obtained:

$$k_s^2 \cong k_{TF}^2/\left(1 + \tfrac{9}{4}\theta^2\right)^{1/2}. \tag{18}$$

This yields an expression for the screening constant of quantum plasmas that applies for all degrees of degeneracy. For $k_BT \ll E_F$ it reduces to k_{TF}, while for $k_BT \gg E_F$ it yields k_D.

A clear way to illustrate the transition from collective to individual behavior is shown in Fig. 1, where we plot the energy-loss function (ELF) as a function of ω for a set of values of the ratio q/k_s: 0.2, 03, 0.5, and 0.7, as indicated in the figure. In Figs. 1(a) and 1(b) we show the ELF function for very different plasma conditions: (a) density $n = 10^{15}$ cm^{-3}, $T = 10^8$ K, and (b) $n = 10^{23}$ cm^{-3}, $T = 10$ eV. These plasma parameters are appropriate for the cases (a) low-density nondegenerate plasma such as in a Tokamak device, and (b) high-density partially degenerate plasma ($k_BT \approx E_F$) in the range of interest for ICF experiments.

As may be observed, for $q/k_s < 0.3$, the ELF function has the shape of a very narrow plasma resonance and becomes increasingly wide for $q/k_s > 0.3$, indicating the onset of the Landau damping phenomenon [44]. We have found that this behavior is reproduced through a very wide range of densities and temperatures.

Therefore, we conclude that the appropriate value to separate the domains of collective and individual behavior may be set for a wide range of plasma conditions at $q_c = 0.3\ k_s$.

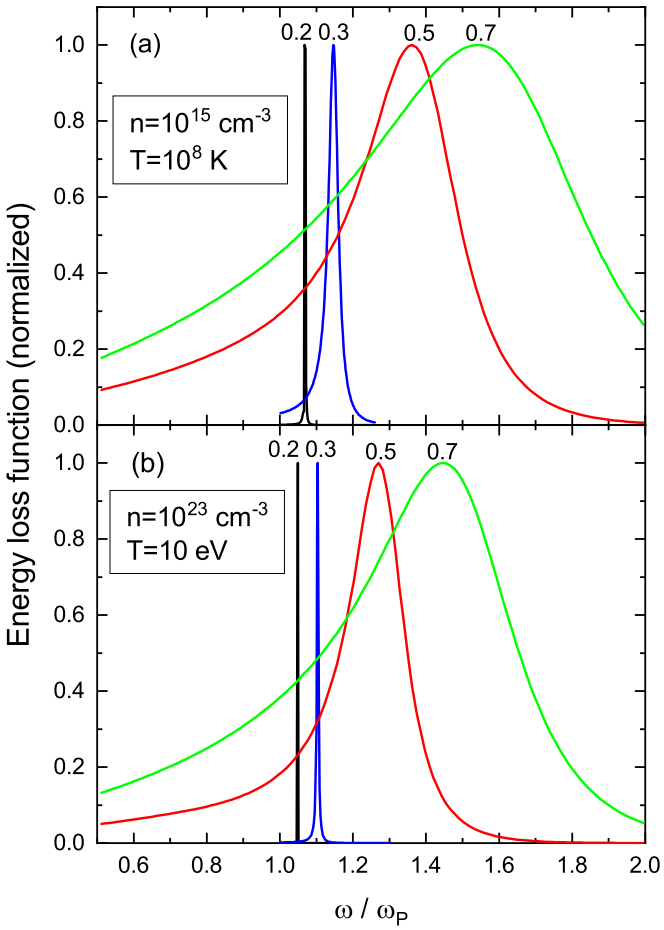

FIG. 1. Energy-loss function for four different values of q with two different plasma densities and temperatures.

IV. REGIONS OF INTEGRATION

As stated in Eqs. (10)–(12), the ω integrals comprise regions of positive and negative frequencies with limits given by the values of $\omega_{\min}$ and $\omega_{\max}$, Eqs. (7) and (8). To illustrate the cases of interest we show in Fig. 2 the regions of integration, delimited by the curves $\omega_{\min}$ and $\omega_{\max}$. Figure 2(a) corresponds to the case of protons (considered here as infinite-mass particles), and Fig. 2(b) to the case of positrons or electrons, with mass m_e. (Notice that the wave vectors q and k will be used indistinctly in the following.)

This figure shows the symmetry of the integration regions I and II for protons and an important asymmetry for the other two particles. In particular, in the latter case, represented by Fig. 2(b), the integration on region I ($\omega < 0$) extends to a maximum wave vector value $q_{\max}^{(1)} = 2m_ev/\hbar$ (indicated by a solid dot in the figure), whereas the integration range for region II ($\omega > 0$) extends to infinity. This region is separated in two subregions: IIa ($0 < q < 2m_ev/\hbar$) and IIb ($2m_ev/\hbar < q < \infty$).

The contributions of these regions are strongly affected by the properties of the $N(\omega)$ function. As will be shown, this leads to significant new effects.

The general expressions for the various energy-loss moments were given in Sec. II. A question of interest here is to analyze separately the contribution of loss and gain processes, i.e., $Q^{(n)} = Q^{(n)}_{\text{loss}} + Q^{(n)}_{\text{gain}}$. Considering the differences in the integration regions shown in Fig. 2, we obtain different expressions for heavy (protons) or light (positrons, electrons) particles.

In the case of protons, with mass $m_p \gg 1$ ($m_p \to \infty$)

$$Q^{(n)}_{\text{loss}}\big|_{\text{protons}} = \frac{2}{\hbar\pi}\left(\frac{Ze}{v}\right)^2 \int_0^\infty \frac{dq}{q} \int_{\omega_{\min}(q,v)}^0 (\hbar\omega)^n N(\omega) \times \text{Im}\left[\frac{-1}{\varepsilon(q,\omega)}\right] d\omega, \tag{19}$$

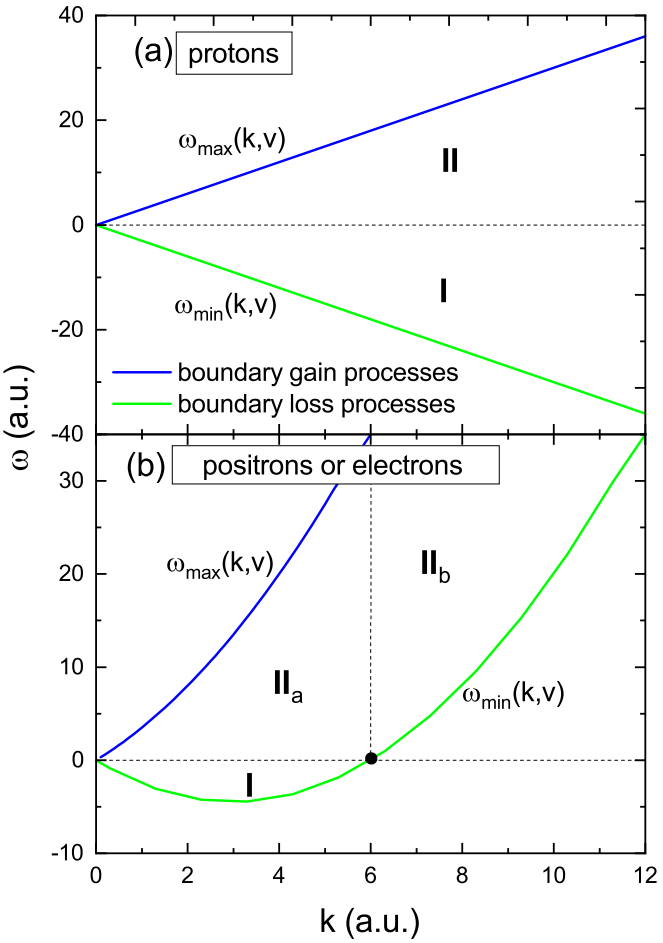

FIG. 2. Integration regions for the energy-loss function in the plane k, ω (values in atomic units). The dot at $k = 6$ in panel (b) indicates the value of $q_{\max} = 2m_e v/\hbar$ for this particular case ($v = 3$ a.u.) and corresponds to the limit of the q integrals in Eqs. (21)–(23).

$$Q^{(n)}_{\text{gain}}\big|_{\text{protons}} = \frac{2}{\hbar\pi}\left(\frac{Ze}{v}\right)^2 \int_0^\infty \frac{dq}{q} \int_0^{\omega_{\max}(q,v)} (\hbar\omega)^n N(\omega) \times \text{Im}\left[\frac{-1}{\varepsilon(q,\omega)}\right] d\omega \tag{20}$$

whereas for light particles the integration on region I has a maximum q value, $q_{\max} = 2m_e v/\hbar$ (cf. Fig. 2):

$$Q^{(n)}_{\text{loss}}\big|_{I} = \frac{2}{\hbar\pi}\left(\frac{Ze}{v}\right)^2 \int_0^{2m_e v/\hbar} \frac{dq}{q} \int_{\omega_{\min}(q,v)}^0 (\hbar\omega)^n N(\omega) \times \text{Im}\left[\frac{-1}{\varepsilon(q,\omega)}\right] d\omega, \tag{21}$$

and the integral on region II splits in two terms, II_a and II_b, with different integration limits in q and ω given by

$$Q^{(n)}_{\text{gain}}\big|_{\text{IIa}} = \frac{2}{\hbar\pi}\left(\frac{Ze}{v}\right)^2 \int_0^{2m_e v/\hbar} \frac{dq}{q} \int_0^{\omega_{\max}(q,v)} (\hbar\omega)^n N(\omega) \times \text{Im}\left[\frac{-1}{\varepsilon(q,\omega)}\right] d\omega, \tag{22}$$

$$Q^{(n)}_{\text{gain}}\big|_{\text{IIb}} = \frac{2}{\hbar\pi}\left(\frac{Ze}{v}\right)^2 \int_{2m_e v/\hbar}^\infty \frac{dq}{q} \int_{\omega_{\min}(q,v)}^{\omega_{\max}(q,v)} (\hbar\omega)^n N(\omega) \times \text{Im}\left[\frac{-1}{\varepsilon(q,\omega)}\right] d\omega. \tag{23}$$

When applying these considerations great differences are obtained in the results for different particles, such as protons, positrons or electrons. We will describe in the next section each of these cases in detail.

A. Collective excitations

As noticed before the variables q and k may be used indistinctly. In this section we prefer to use the variable k to distinguish plasmon resonances characterized by line integrals from nonresonant contributions characterized by double integrals on the q-ω plane.

As indicated before, from the analysis of the ELF we can separate two characteristic regions: $k < q_c$ and $k > q_c$, such that in the first region the ELF takes the form of a narrow resonance, corresponding to the excitation of collective modes (called plasmons in the quantized descriptions [53]), and the region $k > q_c$ corresponds to excitations of individual electrons. First, we can isolate the plasmon contribution by representing the resonance in the form [41]

$$\text{Im}\left[\frac{-1}{\varepsilon(k,\omega)}\right] = \frac{\pi}{D(k)}[\delta(\omega-\omega_k) - \delta(\omega+\omega_k)], \tag{24}$$

where

$$D(k) = \left|\frac{\partial \varepsilon_1(k,\omega)}{\partial\omega}\right|_{\omega=\omega_k}. \tag{25}$$

An approximate expression that may be useful in some cases—for instance, in the plasmon-pole approximation [47]—is $D(k) \approx 2\omega_k/\omega_p^2$.

Now, to perform the calculations a knowledge of the dispersion relation for the resonance frequency ω_k is needed. Various approximations can be used [9,42,54]; in particular, an accurate numerical study of the plasma resonance was made in Ref. [17], where the following fitting formula was obtained:

$$\omega_k = \omega_p(a_0 + a_1 x + a_2 x^2 + a_3 x^3), \tag{26}$$

where $x = k/k_s$ and the values of the coefficients are $a_0 = 1$, $a_1 = 0.3$, $a_2 = 1.2$, $a_3 = -0.45$. This provides a useful analytical expression that may be used in numerical integrations.

Let us consider, for definiteness, the particular case of the stopping power, namely,

$$S = -Q_1 = -\frac{2}{\pi}\frac{(Ze)^2}{v^2}\int_0^\infty \frac{dk}{k}\int_{\omega_{\min}}^{\omega_{\max}} \omega N(\omega) \times \text{Im}\left[\frac{-1}{\varepsilon(k,\omega)}\right] d\omega. \tag{27}$$

Replacing here the expression of Eq. (24) we get

$$S_{\text{pl}} = \frac{2}{\pi}\frac{(Ze)^2}{v^2}\int_0^{k_c} \frac{dk}{k}\frac{\pi}{D(k)}\int_{\omega_{\min}}^{\omega_{\max}} \omega N(\omega) \times [\delta(\omega+\omega_k) - \delta(\omega-\omega_k)] d\omega, \tag{28}$$

where $k_c = q_c = 0.3k_s$.

We can separate here the frequency integral in two terms: $I_1(k) - I_2(k)$, where

$$I_1(k) = \int_{\omega_{\min}}^{0} \omega N(\omega)\delta(\omega + \omega_k)d\omega, \tag{29}$$

$$I_2(k) = \int_{0}^{\omega_{\max}} \omega N(\omega)\delta(\omega - \omega_k)d\omega. \tag{30}$$

These integrals are non null only if ω_k is within the range of integration. We can express this property by introducing two Heaviside functions defined by

$$H_1(k, v) = \begin{cases} 1, & -kv + \gamma k^2 < \omega_k < 0 \\ 0, & \text{otherwise,} \end{cases} \tag{31}$$

$$H_2(k, v) = \begin{cases} 1, & 0 < \omega_k < kv + \gamma k^2 \\ 0, & \text{otherwise.} \end{cases} \tag{32}$$

Hence, the integral (28) may be expressed as

$$S_{\text{pl}} = 2\frac{(Ze)^2}{v^2}\int_0^{k_c}\frac{dk}{k}\frac{1}{D(k)}[-\omega_k N(-\omega_k)H_1(k, v) - \omega_k N(\omega_k)H_2(k, v)]. \tag{33}$$

One case of special interest is the case of protons or other heavy particles. In this case we may assume infinite projectile mass ($\gamma = 0$), and so the "recoil effect" (represented by the term γk^2 in the previous equations) disappears. Thus the two Heaviside functions yield the condition $|\omega_k| < kv$.

Moreover, we can use here the property: $N(\omega_k) + N(-\omega_k) = -1$, and so the stopping integral corresponding to plasmon excitations by protons becomes

$$S_{\text{pl}}^{(\text{protons})} = 2\frac{(Ze)^2}{v^2}\int_{k_{\min}}^{k_c}\frac{dk}{k}\frac{\omega_k}{D(k)}. \tag{34}$$

The value of $k_{\min}$ is determined numerically by the intersection of the resonance line ω_k with kv. Thus, in the case of protons the threshold velocity for plasmon excitations is determined by $v_{\text{pl}}^{\text{protons}} = \omega_{k_c}/k_c$. For high energies the value of $k_{\min}$ may be approximated by ω_p/v.

The result of Eq. (34) agrees with the expression (A.5) obtained in Ref. [41]. This shows that for the particular case of protons or other heavy particles the effects of N-processes on the stopping power cancel out (under the approximation $m_p \to \infty$).

Generalizing this result to all energy-loss moments, we get

$$Q_{\text{pl}}^{(n)} = 2\frac{(Ze)^2}{v^2}\hbar^{n-1}\int_0^{k_c}\frac{dk}{k}\frac{\omega_k^n}{D(k)}[(-1)^{n+1}N(-\omega_k) \times H_1(k, v) + N(\omega_k)H_2(k, v)], \tag{35}$$

or, separating the integrals,

$$Q_{\text{pl}}^{(n)} = 2\frac{(Ze)^2}{v^2}\hbar^{n-1}\left[(-1)^{n+1}\int_{k_{\min}^{(1)}}^{k_c}\frac{dk}{k}\frac{\omega_k^n}{D(k)}N(-\omega_k) + \int_{k_{\min}^{(2)}}^{k_c}\frac{dk}{k}\frac{\omega_k^n}{D(k)}N(\omega_k)\right]. \tag{36}$$

Notice that there are two different values of $k_{\min}$ here, corresponding to the intersections of the resonance line $-\omega_k$ with $\omega_{\min}(k)$ in the first case (zone I in Fig. 2) and the intersection of ω_k with $\omega_{\max}(k)$ in the second case (zone II in Fig. 2). In the case of heavy particles, $k_{\min}^{(1)} = k_{\min}^{(2)}$.

When analyzing these contributions it must be kept in mind that in this formulation the "normal" (0-order) energy-loss term comes from the region $\omega < 0$, while in the standard treatment [51,52] the energy loss is conventionally represented by an integral in the region $\omega > 0$. Of course, this is only a question arising from the way the energy-loss and energy-gain regions are defined in the present formulation.

B. Individual excitations

The nonresonant contributions make the most important part of the energy-loss integrals. According to the criterion derived from Fig. 1 of separating collective and individual terms, the nonresonant contributions cover the whole range defined by $q > q_c$ (with $q_c = 0.3k_s$ as obtained in Sec. III). These contributions are described by the double-integral expressions of Eqs. (19)–(23).

To avoid repetition of those particular expressions we may express all these contributions in a unified way in the form

$$Q_{\text{ind}}^{(n)} = \frac{2}{\pi}\frac{(Ze)^2}{v^2}\hbar^{n-1}\left[\int_{q_c}^{q_{\max}^{(1)}} F_{\text{loss}}^{(n)}(q)\frac{dq}{q} + \int_{q_c}^{q_{\max}^{(2)}=\infty} F_{\text{gain}}^{(n)}(q)\frac{dq}{q}\right], \tag{37}$$

where the subscript "ind" refers to the individual (nonresonant) character of these terms.

The F functions here are given by

$$F_{\text{loss}}^{(n)}(q) = \int_{\omega_{\min}}^{0}\omega^n N(\omega)\,\text{Im}\left[\frac{-1}{\varepsilon(q, \omega)}\right]d\omega, \tag{38}$$

and

$$F_{\text{gain}}^{(n)}(q) = \int_{\overline{\omega}_{\min}}^{\omega_{\max}}\omega^n N(\omega)\,\text{Im}\left[\frac{-1}{\varepsilon(q, \omega)}\right]d\omega. \tag{39}$$

In Eq. (37) the wave vector $q_{\max}^{(1)}$ is given by $q_{\max}^{(1)} \approx \infty$ for protons or other heavy particles, and $q_{\max}^{(1)} = 2m_e v/\hbar$ for light particles, which is the value where $\omega_{\min}(k) = 0$ [indicated by a dot in Fig. 2(b)]. The value of $q_{\max}^{(2)}$ is equal to ∞ for all particles. We must remark, however, that these values apply when dielectric functions with a proper quantum behavior are used, but in the case of the classical dielectric function the values of $q_{\max}^{(1)}$ and $q_{\max}^{(2)}$ for heavy particles must be reconsidered for the reasons discussed below.

Additionally, in Eq. (39) we have introduced a lower limit $\overline{\omega}_{\min}$ defined by

$$\overline{\omega}_{\min} = 0 \tag{40}$$

for protons, and

$$\overline{\omega}_{\min}(q, v) = \begin{cases} 0, & q < 2m_e v/\hbar \\ \omega_{\min}(q, v), & q > 2m_e v/\hbar \end{cases} \tag{41}$$

for light particles [corresponding to regions IIa and IIb in Fig. 2(b)].

As indicated before, this compact notation is used here to cast all the expressions of Eqs. (19)–(23) in a unified way and to avoid repetition of particular expressions.

By separating the loss ($\omega < 0$) and gain ($\omega > 0$) terms it will be possible to analyze the contribution of each of them; this will provide interesting insights for the discussion of the results obtained in the following. We notice that each of these integrals can be evaluated straightforwardly, in spite of the divergence of $N(\omega) \sim k_B T/\omega$ at $\omega \approx 0$, because the energy-loss function, $\mathrm{Im}[\frac{-1}{\varepsilon(q,\omega)}]$, becomes linear in ω in this limit. It may also be noticed that, since $\omega_{\max}$ has no upper bound (Fig. 2), the q integral in the range of positive frequencies extends to ∞. In the PWPM the convergence of the integral will be provided by the ELF, due to the Gaussian functions contained in the construction of $\varepsilon(q,\omega)$ in the quantum formulation. However, in the SCL model, the ELF derived in the classical approach does not contain the same convergence property; fortunately, in this case the presence of the Bose function $N(\omega)$ in the integral is the term that assures convergence (in the region $\omega > 0$) due to its exponential decay for large and positive ω.

On the other hand, the convergence of the integral in the region $\omega < 0$ is a more intricate question. For light particles, convergence is obvious since there is a prescribed upper limit $q_{\max} = 2m_e v/\hbar$ (when $\omega < 0$). But in the case of protons or heavier particles there is no upper limit for $q_{\max}$ (assuming infinite mass of these particles). Therefore, in this case a more careful analysis must be made. The convergence property of the Bose function does not apply in this region since $N(\omega) \approx -1$ for large and negative ω. This compromises the convergence of the integral in the SCL approach, but not in the quantum (PWPM) approach where the convergence is assured by the properties of the ELF (as in the positive-ω case described before). As a consequence of this, the q integral in the SCL calculations produces a logarithmic divergence; this is related to a well-known divergent behavior of classical descriptions [32,33]. A way out of this trouble is to insert a cutoff value $q_{\max}$ in a heuristic way [15]. In particular, by choosing $q_{\max} = 2m_e v/\hbar$ the result for the stopping power of protons converges asymptotically to the appropriate Bethe behavior at high velocities [15]. But of course this prescription does not guarantee a correct solution for low velocities [22]. For this reason, the SCL results may show deviations from the correct behavior at low velocities.

V. ANALYSIS AND CALCULATIONS FOR DIFFERENT PARTICLES

As indicated before, the regions of integrations include positive and negative frequencies delimited by the $\omega_{\min}$ and $\omega_{\max}$ curves (Fig. 2). Moreover, in the case of electrons additional conditions arising from the identity of incident and target electrons must be considered. Therefore, it is convenient to consider separately the cases of heavy particles, positrons, and electrons.

A. Heavy particles

We consider first the simplest case of heavy particles. The term "heavy particles" applies here to particles with masses much larger than the electron mass. For these particles the so-called "recoil effect" is negligible. In particular this includes the cases of protons, deuterons, alpha particles, and to a good approximation also muons and pions (see Ref. [55] for quantitative evaluations of recoil effects).

In these cases the second term in the values of $\omega_{\min}$ and $\omega_{\max}$ of Eqs. (7) and (8) may be dropped off and so the extreme values in the ω integrals become $\pm qv$. This corresponds to the straight lines observed in Fig. 2(a).

Let us consider first the expression of the stopping power, Eq. (11), which now becomes

$$S|_{\text{heavy}} = -\frac{2}{\pi}\frac{(Ze)^2}{v^2}\int_0^\infty \frac{dq}{q}\int_{-qv}^{qv} \omega N(\omega)\mathrm{Im}\left[\frac{-1}{\varepsilon(q,\omega)}\right]d\omega. \tag{42}$$

As noticed in Ref. [11] the positive- and negative-frequency contributions may be combined into a single integration over positive frequencies only by using the relation $N(\omega) + N(-\omega) = -1$, and the general property $\varepsilon^*(q,\omega) = \varepsilon(q,-\omega)$ [43,44], which makes the ELF an odd function of ω. This yields the result

$$S|_{\text{heavy}} = \frac{2}{\pi}\left(\frac{Ze}{v}\right)^2\int_0^\infty \frac{dq}{q}\int_0^{qv} \omega\mathrm{Im}\left[\frac{-1}{\varepsilon(q,\omega)}\right]d\omega, \tag{43}$$

which is a well-known expression for the energy loss of heavy particles in plasmas [51,52].

It is of interest to notice that in these cases the stimulated processes [embodied in the factors $N(\omega)$] for positive and negative ω balance each other, so that the final expression does not contain factors $N(\omega)$. Thus, the influence of stimulated processes may be ignored when calculating the stopping power of heavy particles (in the approximation of infinite mass). For this reason previous expressions for the mean energy-loss of heavy particles are retrieved without any modification. This cancellation of assisted gain ($\omega > 0$) and loss ($\omega < 0$) processes can be generalized to all odd-order energy-loss moments, such as for instance the skewness coefficient corresponding to $n = 3$ [56].

We now turn to the calculation of the IMFP and energy straggling, from Eqs. (10) and (12). In this case the presence of even powers of ω changes the parity of the integral with respect to the sign of ω.

Therefore by combining the positive and negative-frequency branches one gets the combination $N(\omega) - N(-\omega) = 2N(\omega) + 1$, which yields integrals over positive frequencies, namely,

$$\frac{1}{\Lambda}\bigg|_{\text{heavy}} = \frac{2}{\hbar\pi}\left(\frac{Ze}{v}\right)^2\int_0^\infty \frac{dq}{q}\int_0^{qv}[2N(\omega)+1] \times \mathrm{Im}\left[\frac{-1}{\varepsilon(q,\omega)}\right]d\omega, \tag{44}$$

and

$$\Omega^2\big|_{\text{heavy}} = \frac{2\hbar}{\pi}\left(\frac{Ze}{v}\right)^2\int_0^\infty \frac{dq}{q}\int_0^{qv}\omega^2[2N(\omega)+1] \times \mathrm{Im}\left[\frac{-1}{\varepsilon(q,\omega)}\right]d\omega. \tag{45}$$

This result was already anticipated in Ref. [11]. The presence here of the factor $[2N(\omega)+1]$ is an important addition with respect to the known expressions for cold targets.

All these expressions receive contributions from the collective and individual ranges of interactions which may be calculated applying the same criterion explained in detail in Sec. 4, i.e., separating the $0 < q < q_c$ (collective) and $q_c < q < \infty$ (individual) contributions, and transforming the first term into a line integral.

Finally, an additional consideration must be made concerning the integration limit of the q integrals when the semiclassical model is used. The classical dielectric function does not have the correct quantum behavior for large ω and q values. For this reason the stopping and straggling integrals (which depend on large ω and q values) have a divergent type of behavior. As it was discussed in the previous section, one way to solve this problem in the SCL calculation is to introduce a cutoff $q_{\max} = 2m_e v/\hbar$ in the q integral [15].

B. Positrons

We consider now the case of positrons. Going back to Eq. (37) and considering in particular the calculation of the stopping power, we split the integral into its $\omega < 0$ and $\omega > 0$ regions, separating the processes of energy loss and energy gain, respectively, $S = S_{\text{loss}} + S_{\text{gain}}$, with

$$S_{\text{loss}} = -\frac{2}{\pi}\left(\frac{Ze}{v}\right)^2 \int_0^{q_{\max}^{(1)}} \frac{dq}{q} \int_{\omega_{\min}(q,v)}^{0} \omega N(\omega) \times \text{Im}\left[\frac{-1}{\varepsilon(q,\omega)}\right] d\omega, \tag{46}$$

$$S_{\text{gain}} = -\frac{2}{\pi}\left(\frac{Ze}{v}\right)^2 \int_0^{\infty} \frac{dq}{q} \int_{\overline{\omega}_{\min}(q,v)}^{\omega_{\max}(q,v)} \omega N(\omega) \times \text{Im}\left[\frac{-1}{\varepsilon(q,\omega)}\right] d\omega, \tag{47}$$

where $\overline{\omega}_{\min}(q, v)$ is given by Eq. (41). In this case the upper limit $q_{\max}^{(1)} = 2m_e v/\hbar$ in the first integral follows naturally from the limit of the integration zone I shown in Fig. 2. By contrast, the integral of Eq. (47) covers the $\omega > 0$ region in Fig. 2 with no upper limit in q or ω.

For the sake of clarity we have shown here the form of the gain and loss expressions for the stopping coefficient; similar expressions can be written for the IMFP and straggling integrals with the only difference of replacing the factor ω in the integrals by 1 or ω^2, respectively.

As in the previous case of protons the q integrals may be separated into collective and individual contributions corresponding to the $0 < q < q_c$ and $q_c < q < \infty$ ranges, applying the different integration schemes indicated in Sec. IV.

C. Electrons

The dynamical restrictions imposed by $\omega_{\min}$ and $\omega_{\max}$ for electrons are equal to those for positrons. However, due to the identity of the external electron with those of the medium, additional restrictions must be imposed [34,38,39], and the integrals become more cumbersome.

Thus, for instance, in the case of incident electrons, the expressions of Eqs. (46) and (47) are replaced by

$$S_{\text{loss}} = -\frac{2}{\pi}\left(\frac{Ze}{v}\right)^2 \int_0^{q_{\max}^{(1)}} \frac{dq}{q} g_x(q) \int_{\omega_{\min}(q,v)}^{0} \omega N(\omega) \times [1 - f_{\text{FD}}(E + \hbar\omega)] H(U_e - \hbar|\omega|) \text{Im}\left[\frac{-1}{\varepsilon(q,\omega)}\right] d\omega, \tag{48}$$

$$S_{\text{gain}} = -\frac{2}{\pi}\left(\frac{Ze}{v}\right)^2 \int_0^{\infty} \frac{dq}{q} g_x(q) \int_{\overline{\omega}_{\min}(q,v)}^{\omega_{\max}(q,v)} \omega N(\omega) \times [1 - f_{\text{FD}}(E + \hbar\omega)] \text{Im}\left[\frac{-1}{\varepsilon(q,\omega)}\right] d\omega, \tag{49}$$

where the factor $g_x(q) = 1 + (\hbar q/m_e v)^4 - (\hbar q/m_e v)^2$ takes into account the exchange effects in the electron-electron interaction due to the identity of the incident and target electrons (i.e., the Ochkur correction) [36,37]; $f_{\text{FD}}(E)$ is the Fermi-Dirac distribution; $E = m_e v^2/2$ is the kinetic energy of the incident electron, and the factor $[1 - f_{\text{FD}}(E + \hbar\omega)]$ serves to exclude those events where the incident electron falls into occupied states after gaining or losing a (positive or negative) energy $\hbar\omega$. This term is important in cases of partial or strong degeneracy, but becomes irrelevant when $k_B T \gg E_F$.

The additional factor $H(U_e - \hbar|\omega|)$ in Eq. (48) requires a more specific explanation. Here $H(x)$ is the step function, so that this term selects only the $\hbar|\omega| < U_e$ range of the ω integral. This condition arises from a proper treatment of exchange effects in the scattering process of identical particles, which, for instance, in the case of high energies, restricts the energy transfer to the range $0 < \hbar|\omega| < E/2$. This follows from the criterion introduced by Bethe [34] of considering as the new primary electron after the interaction the one emerging with the larger energy (cf. also Ref. [35]). Hence, energy transfers larger than a given amount U_e (equal to $E/2$ for high energies [35]) cannot be distinguished from scattering processes where the identity of the interacting electrons is exchanged [34,35]. The extension of this criterion to all energies, where the kinetic energy of the plasma electrons cannot be ignored can be made by introducing an "equipartition energy" $U_e = (E - \overline{E})/2$, where $\overline{E}$ is the mean kinetic energy of plasma electrons [$\overline{E} = (3/2)k_B T$ for classical plasmas]. So that, for an energy transfer $\hbar|\omega| = U_e$, the two interacting electrons will end up with equal energies (assuming the target electron having the average energy $\overline{E}$ before the interaction). And this is the point where the primary and secondary electrons exchange roles.

The Ochkur term $g_x(q)$ provides an approximate way to condense the direct and exchange terms of the electron-electron scattering [36]. As is clear from these considerations, the Ochkur factor, as well as the condition $\hbar|\omega| < U_e$, apply only to the range of individual interactions (i.e., electron-electron scattering), so that both factors $g_x(q)$ and $H(U_e - \hbar|\omega|)$ should be omitted in the calculation of collective excitations. These considerations are akin to those made in Ref. [35] where different treatments are applied to distant and close interactions.

All these considerations illustrate the complexity of describing the effects of identity between incident and target

electrons. The method proposed here is based on previous approximations, some of which, like the Ochkur term, are based on high-energy approximations. Previous studies [39] show that this method compares exceedingly well with experiments in solid targets on a wide energy range. A more in-depth study of the effects of particle identity in electron-electron interactions in plasmas would require further investigations which lie outside the scope of the present study.

For reasons of space we do not include here the expressions for the IMFP and straggling for positrons and electrons, but they are basically equal to those of Eqs. (46)–(49), with the only difference of omitting the factor ω in the IMFP integral and using a factor ω^2 in the straggling integral.

Finally, the same remarks made before on separating the q integrals into collective and individual contributions ($0 < q < q_c$ and $q_c < q < \infty$, respectively) apply here.

VI. CALCULATIONS FOR SPECIAL CASES: HEATED SOLIDS, FUSION PLASMAS, AND STELLAR INTERIORS

A. Plasmas with solid-state densities (heated solids)

The case of very hot plasmas in solids is an example of interest considering the initial stages of heated materials in inertial-confinement-fusion studies. Here we consider as a representative example a plasma characterized by a parameter $r_s = 2$, which corresponds to a typical value of electron density in solids [with the usual relation $(4\pi/3)r_s^3 = 1/n$], and a set of temperatures from 10 to 60 eV. It is of course an unstable system, with temperatures way over the fusion point, but it pertains for instance to intermediate phases in ICF studies.

Calculations of the three main energy-loss moments of protons, positrons, and electrons are shown in Figs. 3–5. The calculations were done using the PWP and SCL models described in Appendix A. In addition, calculations of stopping powers using the exact dielectric function for all plasma degeneracies from Ref. [46], denoted here by AB, are included. Figures 3(a)–5(a) show comparisons between these three approaches. As may be observed, the results of the PWPM are in excellent agreement with those of the AB theory. This serves as a proof of the accuracy of the PWPM approach. The dotted straight lines for low v values in Fig. 3(a) are the analytical low-velocity approximation from Refs. [11,14], namely,

$$S \cong \frac{4}{3}\frac{(2\pi m_e)^{1/2}}{(k_BT)^{3/2}} Z^2 e^4 nv \left[\ln\left(\frac{k_BT}{\hbar\omega_p}\right) + \frac{1}{4}\right], \qquad (50)$$

where $Z = 1$ for protons. This analytical expression applies when $k_BT/E_F \gg 1$ and provides excellent results except for the lower temperature of 10 eV where $k_BT/E_F = 0.8$.

On the other hand, the proton stopping power calculated with the SCL model [Fig. 3(a)] shows important deviations from the correct behavior shown by the PWPM and AB results, both at low and intermediate velocities for the lower temperature of 10 eV, and yields better results as the temperature increases. This behavior may be understood by considering the values of $k_BT/E_F = 0.8$, 2.4, and 4.8 for the three temperatures of this figure. Hence, the performance of the SCL model improves when the plasma degeneracy decreases, as could be expected based on physical

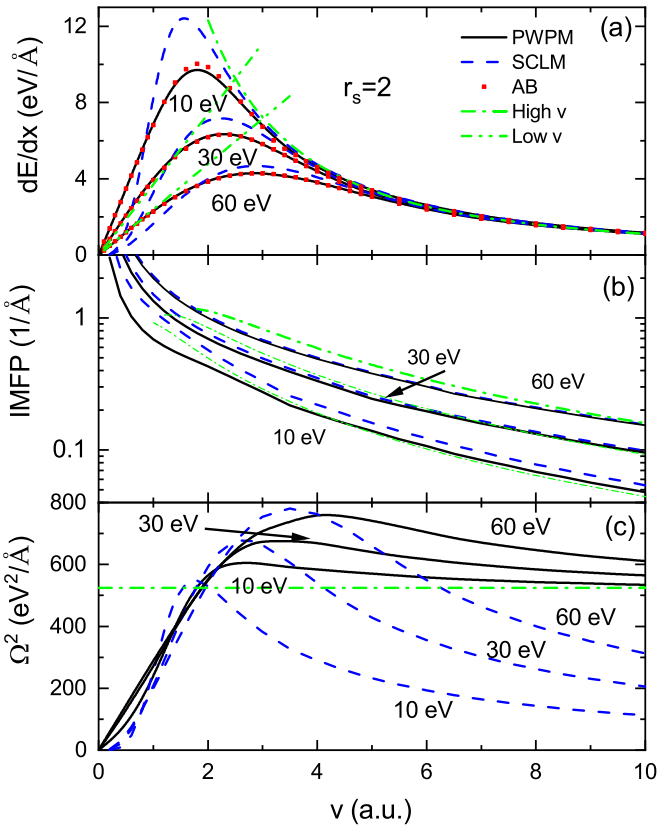

FIG. 3. Energy-loss moments of protons traversing a dense plasma as a function of projectile velocity in atomic units for different temperatures: (a) stopping power, (b) inverse mean-free path, (c) straggling.

considerations. In addition, two further deficiencies of the SCL model in these conditions may be pointed out: the stopping curves deviate from the correct linearity with v at low velocities, and, moreover, the straggling curve shows a decreasing behavior at high speeds [Fig. 3(c)], while the PWPM results converge to the expected Bohr straggling limit [56] given by $\omega_P^2 = 524$ in the units of this figure. The reason why the SCL model fails to reproduce the asymptotic behavior of the straggling is the lack of a proper quantum behavior of the classical dielectric function for large values of q and ω, which are those that dominate the straggling at high energies. As is clear from this figure the PWPM contains the correct quantum properties for all the q-ω range. Hence, the behavior of the straggling serves to test in a very conclusive way the required quantum properties of the dielectric function. Further comments on the failure of the SCL straggling values for high energies will be made in the next section. We conclude from these comparisons that the SCL model does not provide an appropriate description of particle-plasma interactions when the degeneracy parameter k_BT/E_F is close to one. As will be shown below by further calculations the applicability of this model improves greatly when $k_BT \gg E_F$.

It should be noticed here that, in the case $r_s = 2$, nonlinear effects at low velocities may be important for relatively low temperatures [57–59]. Calculations for slow protons in Ref. [59] show stopping power enhancements larger than 10%

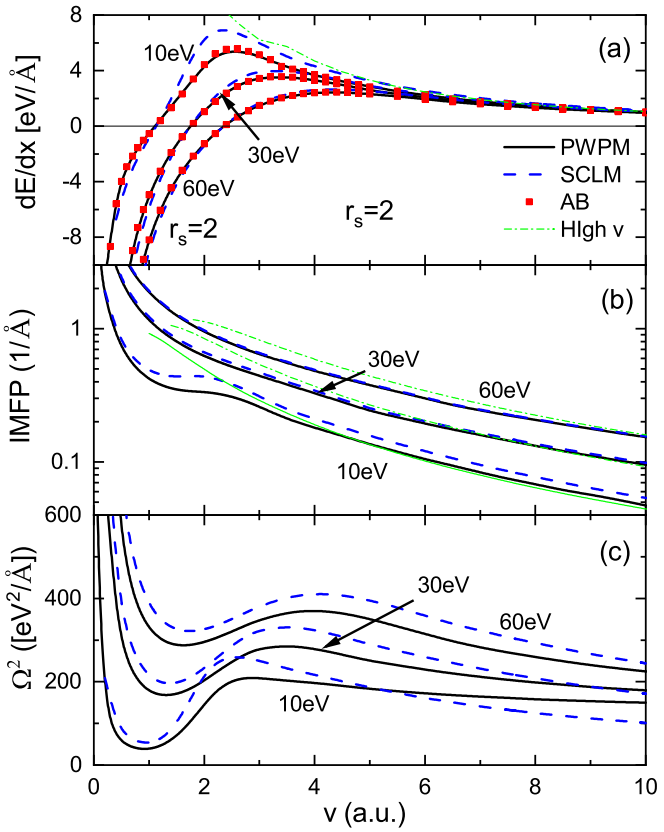

FIG. 4. Energy-loss moments of positrons traversing a solid-state plasma as a function of projectile velocity for different temperatures: (a) stopping power, (b) inverse mean-free path, (c) straggling.

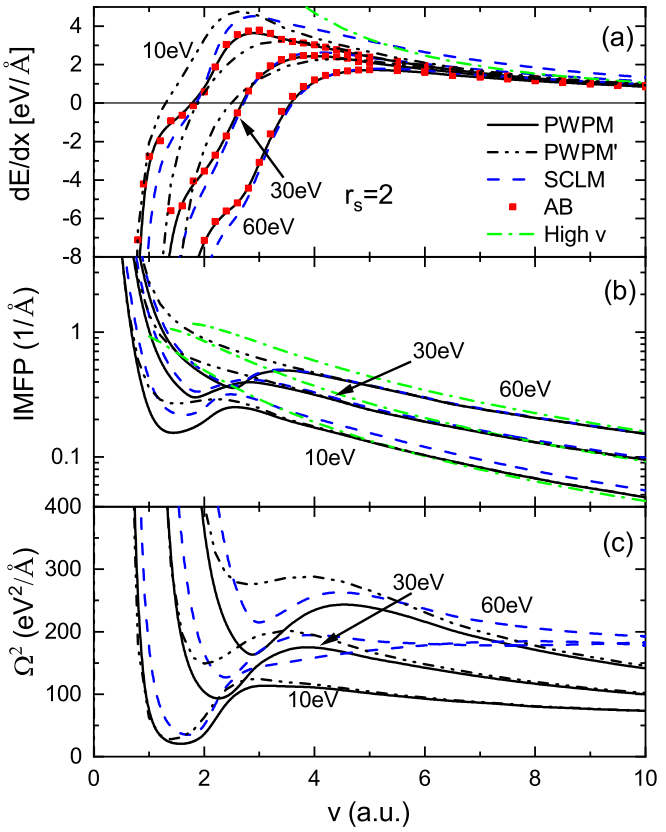

FIG. 5. Energy-loss moments of electrons traversing a solid-state plasma as a function of projectile velocity for different temperatures. Here PWPM is the PWPM calculation without the U_e restriction: (a) stopping power, (b) inverse mean-free path, (c) straggling.

for $\theta < 2$, climbing up to nearly 60% at $\theta = 0$. These nonlinear effects have been studied mostly for cold targets [57].

Another important question already indicated but that should be remarked here is that the calculation of stopping powers with the SCL model require the *ad hoc* introduction of a maximum wave vector $k_{\max} = 2m_e v/\hbar$ in the q integral to avoid a logarithmic divergence, as proposed in Ref. [15]. This particular restriction applies only to the case of protons or heavier particles in the SCL method.

In this respect, an important difference in the calculations for positrons and electrons, in contrast to protons, is that the requirement of an upper cutoff value in the q integral is no longer necessary for the following reasons: the integral in the $\omega < 0$ zone has a natural cutoff at $q = 2m_e v/\hbar$, as indicated by a solid dot in Fig. 2, and the integration over the $\omega > 0$ zone converges regularly due to the exponential decrease of the function $N(\omega)$ when ω tends to infinity. So in this region, where the classical dielectric model lacks a proper quantum behavior, the exponential decline of the $N(\omega)$ function provides a convergent factor.

Finally, we observe that in all cases the high energy decline of the stopping power is consistent with the asymptotic Bethe-like behavior, also shown in the figure, given by

$$S_{\text{high } v} = \frac{B}{v^2} \ln\left(\frac{\alpha_1 m_e v^2}{\hbar\omega_p}\right), \tag{51}$$

where $B = 4\pi n Z^2 e^4/m_e$, and with $\alpha_1 = 2$ for protons, 1 for positrons, and $0.5\sqrt{e/2} = 0.583$ for electrons [34,35].

Regarding the case of positrons, shown in Fig. 4, interesting differences with the case of protons are observed. First, the stopping power drops to negative values in the range of low velocities, and at the same time the IMFP and the straggling values show a divergent behavior. A similar behavior is found for electrons in Fig. 5. These striking results arise when the energy of the incident particle drops below the corresponding thermal energy of the plasma. This range of energies corresponds to the case of subthermal speeds, which implies that the particle must gain energy from the medium to achieve a final thermal equilibrium. This phenomenon, as well as the curious shapes of the curves for positrons and electrons, will be discussed more specifically in Sec. VII. As noticed, in this range of subthermal energies, the energy straggling becomes very large, which indicates a dominance of energy fluctuations. These fluctuations arise from the large and growing numbers of stimulated loss and gain processes in the interaction of the external particle due to thermal excitations of the medium. As a consequence, the mechanism of slowing down is severely affected by energy exchange processes.

Finally, to show the importance of the energy-transfer restriction imposed by the term $H(U_e - \hbar|\omega|)$ in Eq. (48), we have included in Fig. 5 a set of curves denoted PWMP where this restriction has been eliminated (dash-double-dot lines); in

particular we observe in panel (a) very large shifts in the stopping power curves with respect to the correct (and coinciding) PWPM and AB results. Important differences are observed also in the IMFP and straggling values. In fact, the PWPM curves in Fig. 5 become rather similar to those of positrons in Fig. 4.

As a result of the overwhelming effects of fluctuations that take place in the range of subthermal energies, the image of well-defined particle trajectory is lost, as is also the ideal concept of stopping power of light particles with small velocities moving along straight trajectories. Although it is of interest to show and quantify these effects here for the sake of completeness and comprehension, we stress that the range of main interest for the study of energetic particles in plasmas—such as heating by external ion beams or internally produced 3.5 MeV alpha particles—is primarily well above the range of thermal energies.

As in the previous case of protons, the SCL results for the inverse-mean-free path and energy straggling shown in Figs. 4(b) and 4(c) show significant differences with those of the PWPM for the lower temperature of 10 eV, and better agreement for higher temperatures.

Finally, the green dash-dot lines in Figs. 3(b)–5(b) are theoretical estimations of the IMFP using an approximate expression

$$\left.\frac{1}{\Lambda}\right|_{\rm approx}^{(N)} \cong \left.\frac{1}{\Lambda}\right|_{\rm approx}^{(0)} [2N(\omega_c)+1] \tag{52}$$

where $\frac{1}{\Lambda}|_{\rm approx}^{(0)}$ is the order-0 value of the IMFP calculated with $N(\omega) \to N_0(\omega)$ defined in Eq. (13). Here ω_c is the value of ω_k [Eqs. (24) and (26)] at $k = k_c$, which characterizes the transition from collective to individual excitations.

A useful approximation for $\frac{1}{\Lambda}|_{\rm approx}^{(0)}$ is

$$\left.\frac{1}{\Lambda}\right|_{\rm approx}^{(0)} \cong \frac{\omega_P}{v^2} \ln\left(\frac{\alpha_0 v}{v_s}\right), \tag{53}$$

where $v_s = \hbar k_s/m_e$ and $\alpha_0 \cong 1$ [41].

Although it is a rough approximation, Eq. (52) serves to explain the large increase of the IMFP values (notice the logarithmic scale for the IMFP in Figs. 3–5) produced by a multitude of loss and gain processes. The enhancement factor $[2N(\omega_c)+1]$ applied here is analogous to the term $[2N(\omega)+1]$ in Eq. (44) for protons. The basis for this approximation is the physical assumption that the IMFP is mostly determined by low-q interactions which are localized near the shifted plasma frequency ω_c, in accord with Fig. 1. In this interpretation the cause of the great enhancement of the IMFP is the large number of interactions (loss and gain processes) with energy exchange around ω_c.

This interpretation, however, does not apply to the straggling; the physical reason for the difference between IMFP and straggling is that the former is mostly determined by low-q interactions around ω_P (Fig. 2), and the latter by much more widespread interactions with high-q values, which cannot be represented by a simple $[2(N+1)]$ factor evaluated at a fixed frequency.

We finally notice here that in the calculations of energy losses we have considered the protons as particles with infinite mass, as is usually done in calculations of energy losses of heavy particles [51,52]. This approximation is sustained by the small ratio of electron to proton mass, which implies that in the scale of energies considered here the effects of the finite proton mass are negligible.

B. Fusion plasmas: ICF and Tokamak cases

The most relevant examples of laboratory plasmas are those related to fusion-reactor projects and comprise two very different density ranges. Research on inertial-confinement fusion considers solids compressed and heated to very extreme values (typically densities much larger than normal solid densities, and temperatures in the range of 10^8 K), whereas Tokamak type of plasmas involve electron densities in the range of 10^{15} cm^3, and similarly high temperatures.

We illustrate now the characteristic aspects of the interactions of particle beams with plasmas considering as before the cases of protons, positrons, and electrons. Examples involving positrons are included here for the sake of comparisons although they are not normally produced in these laboratory plasmas but serve to illustrate an intermediate behavior between protons and electrons. For these cases, the high-energy region shifts to higher values of the velocity. Thus we extend the velocity scale in order to display the behavior of the curves up to values of 80 a.u. As shown in previous works [8], for velocities greater than 80 a.u., relativistic effects should be considered.

1. ICF plasmas

To illustrate this case we consider here a plasma characterized by the electron-density parameter $r_s = 1$, i.e., an eightfold increase over normal solid densities. The temperatures of interest in this case are in the range of up to 10 keV ($\cong 10^8$ K).

Figures 6–8 show the results for protons, positrons, and electrons. The results are qualitatively similar to those of $r_s = 2$ shown previously, but we notice here a significant improvement of the SCL results for protons and positrons, in comparison with the reference PWPM values, with the exception of the straggling of protons [Fig. 6(c)], where the SCL model fails at high energies (although the comparison with the PWPM values improves at lower energies). We notice also the excellent agreement in the stopping power and IMFP of protons and positrons. The improvement of the SCL results in these cases is a consequence of the higher values of the parameter $k_BT/E_F \cong$ 20-200. These conditions of low degeneracy are relatively more favorable to the classical dielectric description (with the exception of the range of high-q values where quantum effects become important).

The straggling of protons in Fig. 6 shows a very different behavior in the low- and the high-energy regimes and can be explained by simple arguments. Since in this example the condition $k_BT \gg E_F$ is fulfilled, there is a special relation between the straggling and the stopping power S, valid at low energies ($v < v_T = \sqrt{k_BT/m_e}$), which was obtained in Ref. [11], namely,

$$\Omega^2 \cong 2k_BTS. \tag{54}$$

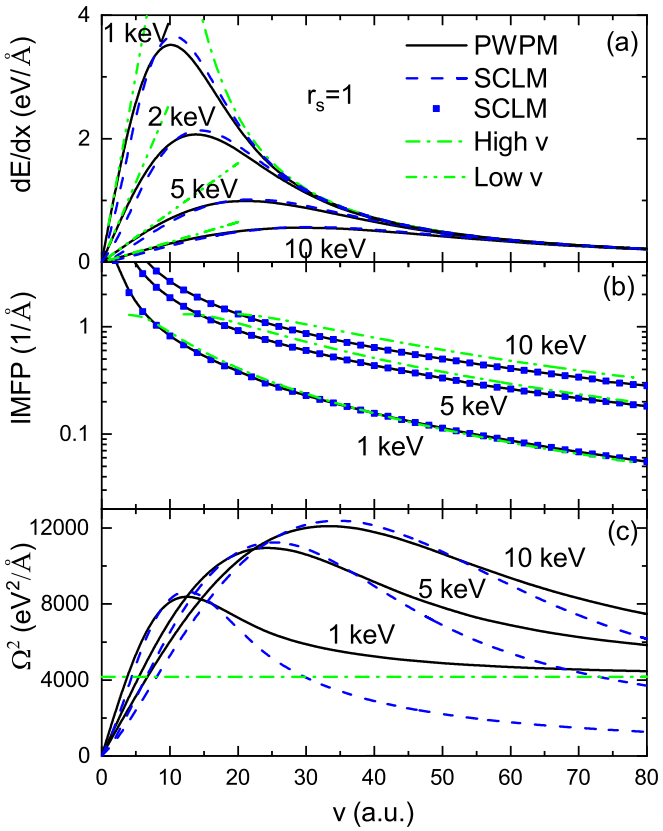

FIG. 6. Energy-loss moments of protons traversing a high-density plasma as a function of projectile velocity for different temperatures: (a) stopping power, (b) inverse mean-free path, (c) straggling.

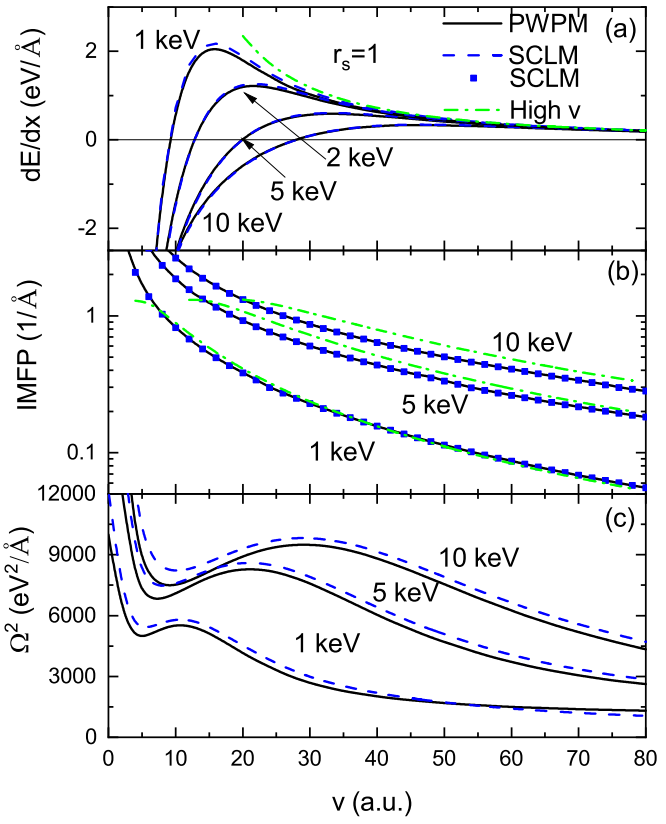

FIG. 7. Energy-loss moments of positrons traversing a high-density plasma as a function of projectile velocity for different temperatures: (a) stopping power, (b) inverse mean-free path, (c) straggling.

Therefore, in these conditions both the stopping power and the energy straggling of protons show a linear dependence on v, as shown in Fig. 6 [and also in two of the curves of Fig. 3(c) where $k_BT/EF = 2.4$ and 4.8]. This is in contrast with the behavior for cold targets where $\Omega^2 \sim v^2$ [60] (notice the curvature of the straggling curve for the lower temperature in Fig. 3(c), where $k_BT/EF = 0.8$, indicating a tendency to a v^2 dependence). The reason for this change in the velocity dependence is just another effect of the Bose term $N(\omega)$, which for $k_BT \gg \hbar\omega$ becomes $N(\omega) \sim k_BT/\hbar\omega$. The factor $1/\omega$ changes the dependence of the integrand in Eq. (45), from ω^2 to ω, i.e., the same form as the stopping integral of Eq. (43). This leads to the simple relation of Eq. (54). On the other hand, the failure of the SCL model in the straggling of protons at high energies has a clear origin: as noticed before, the classical dielectric function does not provide a good description for high-q values, and this failure becomes most notorious in the case of protons, because of the open region of integration shown in Fig. 2, together with the behavior of $N(\omega) \to -1$ for large negative values of ω (region I) which leads to a logarithmic divergence of the stopping integral. This divergent behavior is usually avoided by introducing a maximum cutoff value $k_{\max} = 2m_e v/\hbar$. As explained before, the criterion for choosing this value is to obtain a high-energy behavior of the stopping power in agreement with the Bethe formula. But this cutoff criterion is not satisfactory for the straggling. On the other hand, in the case of positrons and electrons the deficiency of the SCL model for large q and ω is attenuated for the reasons already indicated in the discussion of Figs. 3–5 [i.e., the convergent behavior of the factor $N(\omega)$ in region IIb of Fig. 2].

Finally, Fig. 8 shows the results for electrons. Here, and by comparing with the results for positrons in Fig. 7, important differences due to the special restrictions (produced by the electron identity) are observed. Moreover, the SCL method shows significant deviations from the PWPM behavior. As a new feature, the curious drops in the values of the IMFP in Fig. 8(b) are produced by the competition between gain and loss terms, and are "in phase" with similar drops in the straggling curves.

2. *Tokamak plasmas*

The behavior of the energy-loss coefficients in Tokamak-type plasmas is illustrated in Fig. 9, where we show a set of calculations for a plasma density $n = 10^{15}$ cm^{-3}, and temperature 10^8 K. An important difference with the cases calculated before is the very large value of the parameter $k_BT/E_F = 2.4\times10^8$. This is an example of a fully nondegenerate high-temperature plasma. It is then expected that the classical description should work here quite well.

Figure 9(a) shows an impressively good agreement in the stopping power values calculated with the PWPM and SCLM

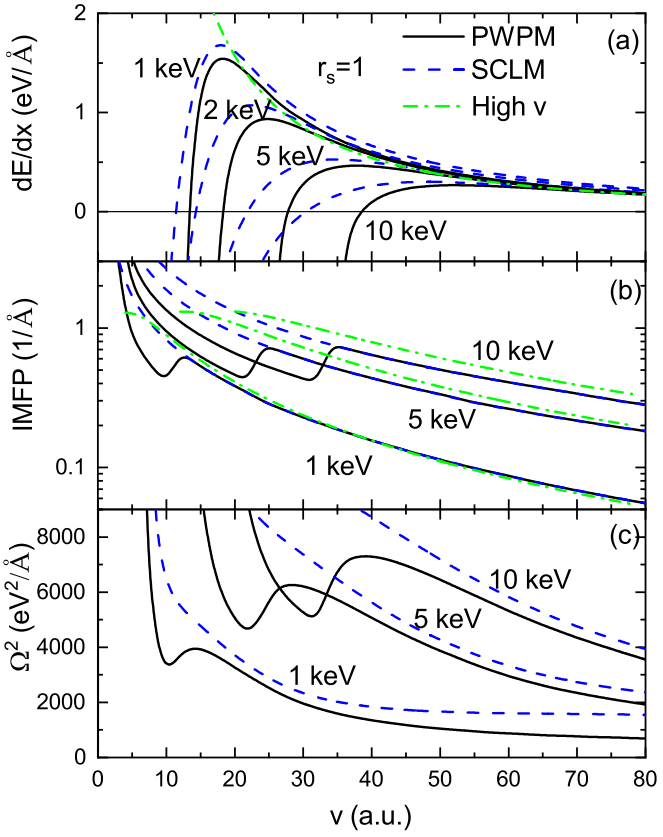

FIG. 8. Energy-loss moments of electrons traversing a high-density plasma as a function of projectile velocity for different temperatures: (a) stopping power, (b) inverse mean-free path, (c) straggling.

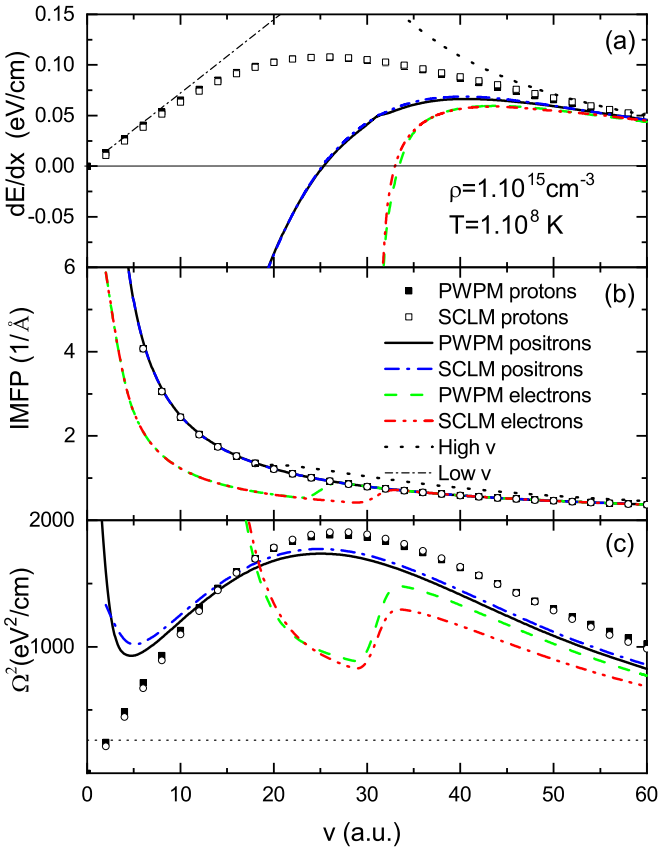

FIG. 9. Energy-loss moments of protons, positrons, and electrons traversing a plasma as a function of projectile velocity for a characteristic temperature corresponding to Tokamak conditions. High- and low-v limits are shown for protons: (a) stopping power, (b) inverse mean-free path, (c) straggling.

for all the particles. In the same way, Fig. 9(b) shows excellent agreement for the IMFP of protons and positrons over the whole energy range, while the IMFP of electrons also shows excellent agreement between the two dielectric models, except only for an intermediate range of velocities (between about 25 and 35 a.u.) where a short misadjustment occurs. Finally, the straggling of protons shown in Fig. 9(c) goes to zero when $v \to 0$; this behavior is consistent with the behavior of the straggling of protons already observed for the cases of $r_s = 1$ and 2. Instead, the results for positrons and electrons show the same type of divergent behavior for lower values of v as in the previously studied cases. Further explanations of this behavior are given in Sec. VII where we analyze the contributions of the $\omega < 0$ and $\omega > 0$ regions of Fig. 2.

C. Stellar interiors: The sun

The extreme conditions that characterize the stellar interiors provide other relevant systems that serve to test the new effects on the interactions described here. To take a most familiar example we consider here the case of the solar interior, and more particularly the most stringent conditions at and around the sun center, characterized by temperatures and densities of 1.6×10^7 K and 160 g/cm^3, respectively, and consisting of ≈75% hydrogen and 25% helium. This yields a total electron density of 8.4×10^{25} cm^{-3}.

The results for the energy-loss moments of the same test particles for this case are shown in Fig. 10.

This figure shows similarities with Fig. 9 corresponding to the Tokamak example, so that most of the comments made earlier on that figure apply also here. We notice, however, important differences in the magnitudes of the stopping power and straggling values, while surprisingly the IMFP values have similar magnitudes. These features may be readily explained by the differences in densities and temperatures for the two media. In the case of the stopping power, a straightforward estimation can be made by using the low-energy expression of Eq. (50). Inserting in this equation the values of density and temperature and the corresponding values of k_BT/ω_p (4.1 and 7.3×10^6 for the sun and the Tokamak cases considered here) we get a stopping power ratio $S_{\rm sun}/S_{\rm Tokamak} = 1.3\times10^{11}$. This estimation compares well with the ratio of stopping powers shown in Figs. 9 and 10 for velocities in the low-energy range and even around the stopping power maximum. Of course the main difference is produced by the much higher solar density.

By a similar argument we may explain the large difference in the straggling values, considering in particular the Bohr limit in the case of protons, which is directly proportional to the electron density, so that a ratio of the order of 10^{11} is

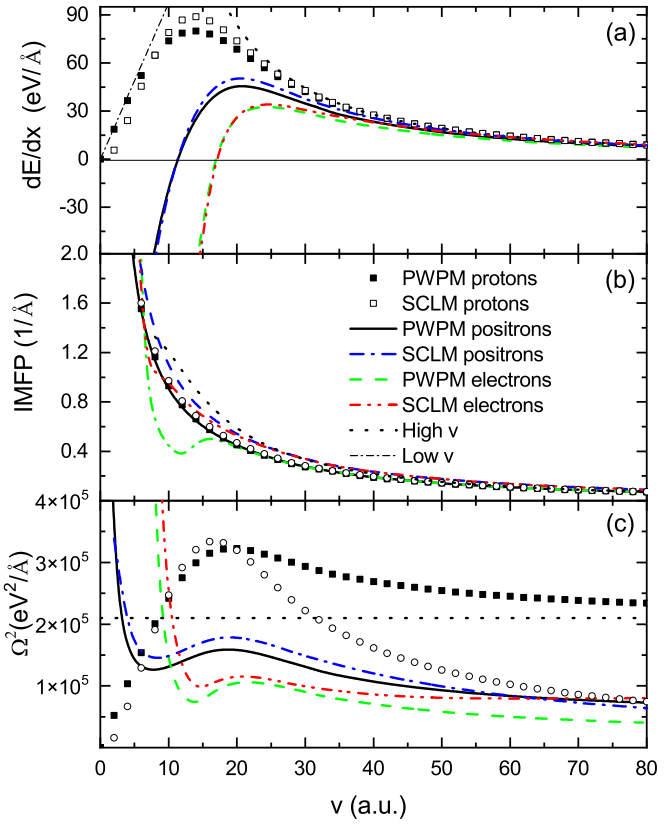

FIG. 10. Energy-loss moments of protons, positrons, and electrons traversing a plasma as a function of projectile velocity for a characteristic temperature corresponding to solar interior conditions: (a) stopping, (b) inverse mean-free path, (c) straggling.

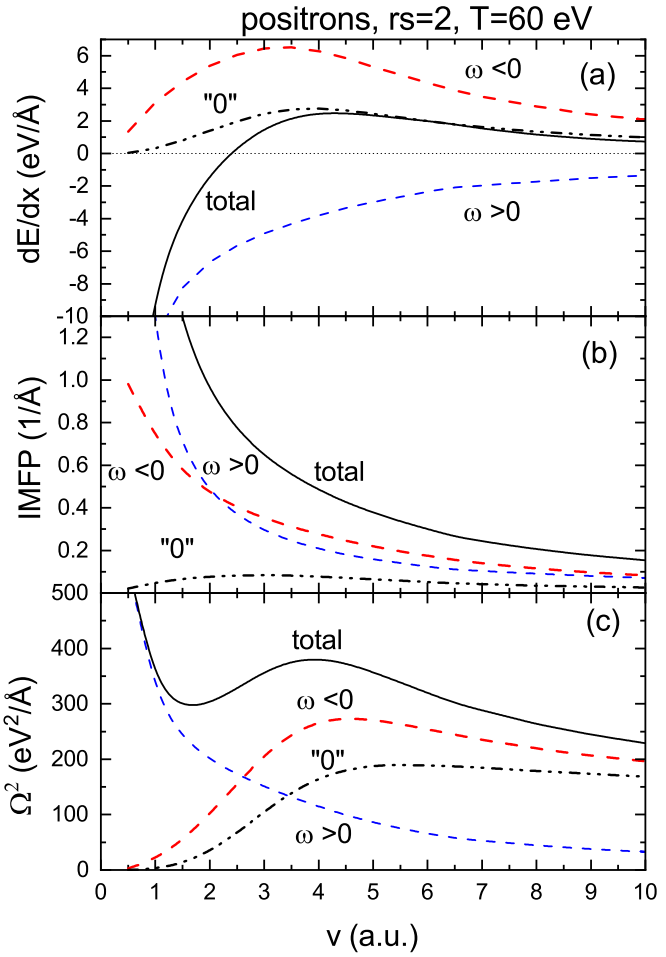

FIG. 11. Contributions to the energy-loss moments as a function of projectile velocity for positrons traversing a solid-state plasma with $r_s = 2$ and a characteristic temperature $T = 60\,\text{eV}$. High- and low-v limits are shown for protons. Panel (a) shows stopping power, panel (b) shows inverse mean-free path, and panel (c) shows straggling. In all cases, dashed-dot-dot lines show the result for a cold plasma, i.e., $T = 0$.

obtained, again in good agreement with the ratio between the straggling results in these two figures.

Finally, considering these big differences in the stopping and straggling values, it is surprising that the values of the IMFP in Figs. 9 and 10 have such similar magnitudes. This similarity can be explained from Eqs. (52) and (53). These expressions show that the IMFP scales basically as $\omega_p N(\omega_p)$. Moreover, when $k_B T/\omega_p \gg 1$, the Bose factor can be approximated by $k_B T/\omega_p$, which yields the simple scaling criterion IMFP $\sim k_B T$. Then, considering the temperature ratio: $10^8/(1.6\times10^7) \approx 6$ we may expect a larger IMFP for the Tokamak but maintaining roughly the same order of magnitude.

Hence, we have here an example where three different scaling properties are observed, the straggling Ω^2 that scales with the density, the IMFP that scales with the temperature, and the stopping power that scales with a combination of density and temperature. This arguments explain very satisfactorily, on a qualitative basis, the quite different scaling properties observed when comparing these two figures.

VII. ANALYSIS AND DISCUSSION: LOSS AND GAIN PROCESSES

All the cases studied before provide illustrative examples of the characteristics and modifications of the energy-loss coefficients as a result of the interactions of external test particles with the electronic excitations of a plasma. Much of the new effects arising from the so-called N-processes have already been illustrated here in rather global ways. But we consider useful and perhaps even necessary to provide some additional insight on the way these processes work through statistically assisted gain and loss terms in the energy exchange between the external particle and the plasma. These different processes occur in the positive and negative domains of frequencies illustrated in Fig. 2. So to obtain a more comprehensive view of this question it is appropriate to analyze these contributions separately.

Here we take by way of example the case of positrons, which serves to illustrate more clearly the effects. Thus, we show in Fig. 11 the contributions of the $\omega < 0$ and $\omega > 0$ regions to the three energy-loss coefficients for positrons in a plasma characterized by $r_s = 2$ and temperature $T = 60\,\text{eV}$. Figure 11(a) shows very clearly the competing effects between gain and loss processes in the stopping power. For velocities larger than about 3 a.u., the energy-loss

component ($\omega < 0$) dominates and produces a final stopping power (black solid line) with a "normal" behavior, going to the expected Bethe limit at high velocities. Conversely, at lower energies the energy-gain term ($\omega > 0$) yields large negative stopping values and dominates over the loss term; as a result, the total energy loss crosses the zero line and sinks with a divergent-type behavior. As noticed before, there is a clear physical meaning for this behavior: when the kinetic energy of the test particle becomes subthermal the particle must gain energy from the plasma in order to achieve the final conditions of thermal equilibrium. The curve identified by "0" in this figure is the calculation of order-0 according to Eq. (14), which corresponds to neglecting the statistical effects of the Bose terms $N(\omega)$ (i.e., the so-called N-processes). Hence, this figure illustrates very clearly the two distinct effects produced by the condition of statistical equilibrium in the interaction of the external particle with the excitations of the medium.

Figure 11(b) shows the contributions to the IMFP. In this case the gain and loss terms show a similar divergent behavior, producing a total IMFP with similar characteristics, in sharp contrast with the expectations derived from the 0-order calculation. Finally, Fig. 11(c) shows the corresponding contributions to the energy straggling. This explains the very unexpected change in the straggling curves observed in all previous figures corresponding to positrons and electrons. In this case the loss term ($\omega < 0$) shows a rather "normal" behavior (similar to the 0-order term), but at low energies the gain term ($\omega > 0$) takes over, with a very large increase (owing to growing energy-loss fluctuations) and produces the anomalous change of behavior of the final straggling curve. The modulation of the straggling curve of positrons and electrons is therefore a consequence of the competition between gain and loss processes. These effects are potentiated in the case of electrons by the special restrictions that diminish the contribution of the loss ($\omega < 0$) terms.

An overflying question here is why the effects of statistical equilibrium manifest in so different ways in these three energy-loss coefficients. The explanation comes from the fact that the corresponding integrals weight in different ways the low- and high-energy contributions (through the different power of ω in the integrals). The IMFP is dominated by low-energy excitations (distant interactions) while the opposite occurs for the straggling; the intermediate behavior is found in the stopping power, which keeps a moderate balance between low- and high-energy excitations (in accord with Bohr's partition rule for fast particles [56]). In all cases the most extreme behavior is observed in the $\omega > 0$ contribution; this is a result of the wide and open integration region II displayed in Fig. 2, which covers all the extreme ranges (from the low-q and -ω to the high-q and -ω region).

VIII. SUMMARY AND CONCLUSIONS

As indicated in the Introduction, the purpose of this work was to provide a general framework for the study of quantum statistical effects in the interaction of test particles with classical and quantum plasmas in conditions of thermal equilibrium.

To this end, we developed in detail the formulation of the interaction process and made a comprehensive study of the above-mentioned effects, considering the cases of heavy and light particles, and performing a set of calculations of the three most relevant energy-loss moments, namely, stopping power, energy straggling, and inelastic mean-free path. We analyzed a set of cases of central interest for current fusion projects and stellar interiors of astrophysical interest, considering in particular the conditions at the sun's core.

The new findings that arise from this study may be summarized as follows:

(i) The processes of energy exchange between the test particle and the plasma receive competing contributions from gain and loss processes, governed by the Bose function $N(\omega)$, which may produce large effects on all the energy-loss coefficients.

(ii) We provided a well-defined scheme to separate collective and individual contributions (from a careful study of the behavior of the energy-loss function), and formulas to evaluate the collective terms in the form of line integrals.

(iii) In the case of heavy particles (protons, alpha particles, or heavier ions) we obtain a nearly exact cancellation of assisted terms (here called N-processes), corresponding to gain and loss contributions to the stopping power. As a result of this, the stopping power coincides with the well-known and widely used expression found in the literature and represented here by the 0-order term [Eq. (43)]. This cancellation property can be generalized to all the odd-order moments of the energy loss. (We notice, however, that this cancellation becomes exact only in the infinite-mass approximation.)

(iv) We find a very large enhancement of the IMFP and straggling coefficients for heavy particles, with growing magnitude at low velocities. This effect may be explained as a consequence of fluctuations in the interaction process produced by the large number of thermally activated electronic excitations. We find an approximate scaling expression for the enhancement of the IMFP of the form $[2N(\omega_c) + 1]$, where $N(\omega)$ is the Bose function that regulates the number of thermal excitations in the plasma.

(v) In the case of light particles, such as electrons and positrons, the stopping power shows an unusual (but physically expected) change of behavior, turning to negative values at low velocities. This phenomenon has a clear physical interpretation: for energies of the test particle lower than the thermal speed of plasma electrons the particle gains energy from the plasma as a way to achieve a final thermal equilibrium. This effect has already been exposed but in a more restricted way [32,33]. This change from the regular behavior is also expected for heavy particles but it occurs for velocities much lower than those of interest for this study.

(vi) Also for such light particles, we obtain a pronounced enhancement in the IMFP and straggling coefficients, similar to those obtained for heavy particles and of similar origin.

(vii) We gave special consideration to the case of electrons as incident particles, showing the importance of the restrictions imposed by the identity principle (with respect to target electrons), an aspect that has not been taken into account before in the case of plasmas.

Another aspect investigated in the present study is the question of the applicability of the classical dielectric function to describe the energy-loss moments for the cases of light and heavy particles and for the different plasma

conditions considered here. The results obtained here show that

(viii) The semiclassical approach, consisting in the use of a classical dielectric function and the full quantum statistical formulation, provides very good results for the stopping power of heavy particles when a cutoff prescription in the momentum transfer is applied.

(ix) This procedure yields fairly good results in some cases and fails in others (in particular for the straggling of protons), as illustrated by the various examples considered here. It can be noticed that the SCL approach yields good results for high temperatures and low densities, such that $k_BT \gg E_F$ (as in the example of Tokamak plasmas). These are in fact the conditions where the SCL approach may be expected to work best.

(x) On the other hand, the so-called wave-packet model, built in terms of Gaussian functions in the formulation previously developed by Kaneko [48–50] and extended to quantum plasmas in Ref. [47], yields excellent results in all cases when compared with the more exact dielectric function of Ref. [46].

As a general conclusion of this study, the quantum statistical formulation for particle-plasma interactions presented here can be extensively applied over wide ranges of plasma conditions.

We finally note that previous theoretical studies where the effects of statistically assisted processes of energy exchange, or the special restrictions for incident electrons, were not taken into account, may have to be reconsidered.

ACKNOWLEDGMENTS

This work was supported by the following institutions of Argentina: Consejo Nacional de Investigaciones Científicas y Técnicas, Agencia Nacional de Promoción Científica y Tecnológica, and Universidad de Buenos Aires.

APPENDIX A: DIELECTRIC FUNCTIONS

This Appendix summarizes three main formulations of the dielectric function for a plasma: (a) an exact quantum formulation for plasmas of arbitrary degeneracy (AB formulation) [46], (b) a quantum formulation based on Gaussian functions (PWP formulation) [47], and (c) the classical formulation for the Maxwell-Boltzmann distribution of electron speeds (SCL formulation) [42]. The derivations of all these cases are based on the theoretical developments of Ref. [46].

1. The quantum dielectric function

The three dielectric models described here may be derived from the general expression [46]:

$$\epsilon(q,\omega) = 1 + \frac{e^2}{\pi^2 q^2}\int d^3k\, \frac{f_{\rm FD}(\overrightarrow{k}+\overrightarrow{q}) - f_{\rm FD}(\overrightarrow{k})}{\hbar\omega + i\delta - (E_{\overrightarrow{k}+\overrightarrow{q}} - E_{\overrightarrow{k}})}, \tag{A1}$$

where $E_{\overrightarrow{k}} = \hbar^2k^2/2m_e$, and $f_{\rm FD}(\overrightarrow{k})$ is the Fermi-Dirac distribution function for plasmas of arbitrary degree of degeneracy:

$$f_{\rm FD}(\overrightarrow{k}) = \{1 + \exp[\beta(E_k - \mu)]\}^{-1}, \tag{A2}$$

where $\beta = 1/k_BT$, and μ is the chemical potential of the plasma. The chemical potential may be determined with the Fermi-Dirac integral of order 1/2 using Eq. (6) of Ref. [46].

Closed expressions for the real and imaginary parts of $\epsilon(q,\omega)$ can be obtained from Eq. (A1). The real part may be written as [46]

$$\varepsilon_1(q,\omega) = 1 + \frac{\chi_0^2}{4z^3}[g(u+z) - g(u-z)]. \tag{A3}$$

Here $\chi_0^2 = (1/\pi k_F a_0)$, $a_0 = \hbar^2/m_e e^2$ is the Bohr radius, $\theta = 1/D = k_BT/E_F$, E_F is the Fermi energy, $\eta = \mu/k_BT$, and

$$g(x) = \int_0^\infty \frac{y\,dy}{1 + e^{Dy^2-\eta}} \ln\left|\frac{1+x}{1-x}\right| \tag{A4}$$

in terms of the reduced variables: $u = \omega/qv_F$, $z = q/2k_F$.

The expression for the imaginary part is

$$\varepsilon_2(q,\omega) = \frac{\pi\chi_0^2}{8z^3}\theta \ln\left[\frac{1+\exp[\eta-(u-z)^2/\theta]}{1+\exp[\eta-(u+z)^2/\theta]}\right]. \tag{A5}$$

The dielectric function obtained in this way provide the exact solution for the linear response of the electron gas at finite temperatures (in the RPA approximation [7]), and serves as a reference model of comparison for other approximations. It will be referred to here as the AB formulation according to the complete study provided in Ref. [46].

In the following we obtain particular expressions for the case $\theta \gg 1$, including the quantum-Gaussian approach and the fully classical case.

2. Quantum dielectric function for Gaussian distributions

A. Analysis of real part

To obtain the expression for Gaussian distributions of electron speeds we consider the limit $\theta \gg 1$ where the function $g(x)$ becomes [Eq. (10b) in Ref. [46]]:

$$g(x) \cong \tfrac{2}{3}D^{1/2}\,\Phi_1(D^{1/2}x), \tag{A6}$$

where $\Phi_1(x')$ is the real part of

$$\Phi(x') = \Phi_1(x') + i\Phi_2(x') = \frac{1}{\sqrt{\pi}}\int_{-\infty}^{+\infty}\frac{e^{-y^2}}{x'-y+i\delta}dy, \tag{A7}$$

with $x' = D^{1/2}x$.

Then Eq. (A3) becomes

$$\varepsilon_1(q,\omega) \cong 1 + \frac{\chi_0^2}{4z^3}\frac{2}{3}D^{1/2}\,[\Phi_1(u'+z') - \Phi_1(u'-z')], \tag{A8}$$

where

$$u' = D^{1/2}u = \frac{\omega}{qv_{2T}}, \quad z' = D^{1/2}z = \frac{\hbar q}{2m_e v_{2T}}, \tag{A9}$$

and v_{2T} is defined by

$$v_{2T} = \sqrt{\frac{2k_BT}{m_e}}. \tag{A10}$$

Note that we are using here the notation $v_T = \sqrt{k_BT/m_e}$, $v_{2T} = \sqrt{2k_BT/m_e}$.

We calculate the factor in Eq. (A8) (with $D = m_e v_F^2/2k_BT$):

$$\frac{\chi_0^2}{4z^3}\frac{2}{3}D^{1/2} = \frac{1}{4\pi k_F a_0}\left(\frac{2k_F}{q}\right)^3\frac{2}{3}\sqrt{\frac{m_e v_F^2}{2k_BT}} = \frac{4\pi ne^2}{\hbar v_{2T} q^3}, \quad \text{(A11)}$$

where $k_F^3 = 3\pi^2 n$, and $v_F = \hbar k_F/m_e$.

Then,

$$\varepsilon_1(q,\omega) \cong 1 + \frac{4\pi ne^2}{\hbar v_{2T} q^3}[\Phi_1(u'+z') - \Phi_1(u'-z')] \quad \text{(A12)}$$

and we notice that

$$u' \pm z' = \sqrt{\frac{m_e}{2k_BT}}\left(\frac{\omega}{q} \pm \frac{\hbar q}{2m_e}\right). \quad \text{(A13)}$$

This is the expression for $\varepsilon_1(q,\omega)$ corresponding to $\theta \gg 1$. It is a quantum-mechanical formula corresponding to Gaussian (Maxwell-Boltzmann) distribution of electron speeds.

As in the Kaneko formulation the function $\Phi_1(x')$ may be calculated from the equivalent formula [49],

$$\Phi_1(x') = \int_0^\infty \sin(x'y)\, e^{-y^2/4} dy, \quad \text{(A14)}$$

which avoids the problem of the pole in Eq. (A7).

Another equivalent expression for this function, useful for numerical calculations, is the following [47]:

$$\Phi_1(x') = 2x' \int_0^1 \exp[x'^2(y^2-1)]dy. \quad \text{(A15)}$$

B. Analysis of imaginary part

The limit of Eq. (A5), when $\theta \gg 1$, was given already by Eq. (28) in Ref. [46], namely,

$$\varepsilon_2(q,\omega) = \frac{m_e\omega_P^2}{\hbar q^3}\left(\frac{2\pi m_e}{k_BT}\right)^{1/2}\sinh\left(\frac{\hbar\omega}{2k_BT}\right) \times \exp\left[-(u^2+z^2)\frac{E_F}{k_BT}\right]. \quad \text{(A16)}$$

The last exponential term may be written more conveniently as

$$\exp\left[-(u^2+z^2)\frac{E_F}{k_BT}\right] = \exp\left\{-\frac{m_e}{2k_BT}\left[\left(\frac{\omega}{q}\right)^2 + \left(\frac{\hbar q}{2m_e}\right)^2\right]\right\}. \quad \text{(A17)}$$

The important difference with the classical expression is that it describes in a correct way the quantum effects in energy-momentum transfers not contained in the classical dielectric function. Therefore, this result it is equivalent to Kaneko's Wave-Packet Model (WPM) [48] adapted to a plasma [47]; it will be referred to here as the Plasma Wave-Packet Model (PWPM). This formulation makes use of all the analytical properties of the original WPM.

Finally, as shown in Ref. [47], this approach may be extended to partially or fully degenerate plasmas using an effective temperature determined in that reference.

3. Classical dielectric function for a plasma ($\theta \gg 1$)

The classical expression for the dielectric function (usually derived from the linearized Vlasov-Poisson equation [43,44]) can now be obtained from Eq. (A1) considering the long-wavelength and low-frequency limit and making the following approximations: $\vec{q} \to 0$, $f(\vec{k}+\vec{q}) - f(\vec{k}) \cong \vec{q}\cdot\vec{\nabla}_k f(\vec{k}) = \hbar\vec{q}\cdot\vec{v}(\partial f/\partial E)$, and $E_{\vec{k}+\vec{q}} - E_{\vec{k}} \cong \vec{q}\cdot\vec{\nabla}_k E_k = \hbar\vec{q}\cdot\vec{v}$

With this approximation one retrieves an expression obtained earlier by Pines [42] in the form

$$\varepsilon(q,\omega) = 1 + \frac{k_D^2}{q^2} W\left(\frac{\omega}{qv_T}\right), \quad \text{(A18)}$$

where $v_T = \sqrt{k_BT/m_e}$, and

$$W(\xi) = W_1(\xi) + iW_2(\xi) = \frac{1}{\sqrt{2\pi}}\int_{-\infty}^{\infty}\frac{x\, e^{-x^2/2}}{x-\xi-i\delta}dx. \quad \text{(A19)}$$

Methods to calculate the function $W(\xi)$ were described long ago by Fried and Conte [61], but we will give here further mathematical expressions useful for straightforward calculations.

It is illustrative to provide here an alternative derivation of this result using the PWPM formulation, which will also yield useful analytical expressions. In this formulation the quantum-mechanical character of ε_1 and ε_2 is given by the terms containing $\hbar$ in Eqs. (A13) and (A17). Therefore, to get the classical result we take the limit $\hbar \to 0$ in those expressions.

Starting from the Φ function of Eq. (A7) we have

$$\Delta\Phi = [\Phi(u'+z') - \Phi(u'-z')] \cong \Phi'(u')\, 2z', \quad \text{(A20)}$$

where Φ' denotes the derivative of Φ.

Let us now define $\Psi(u') = \frac{1}{2}\Phi'(u')$. Taking the derivative of Eq. (A7) we get

$$\Psi(u') = \frac{1}{2}\Phi'(u') = \frac{1}{\sqrt{\pi}}\int_{-\infty}^{\infty}\frac{y\, e^{-y^2}}{y-u'-i\delta}. \quad \text{(A21)}$$

Note that, to obtain this result, a partial integration was applied.

Replacing now $\Delta\Psi$ in Eq. (A12) gives

$$\varepsilon(q,\omega) \cong 1 + \frac{4\pi ne^2}{\hbar v_{2T} q^3}\, 4z'\Psi(u'), \quad \text{(A22)}$$

and replacing $z' = \hbar q/2m_e v_{2T}$ and $v_{2T} = \sqrt{2k_BT/m_e}$, we get

$$\varepsilon(q,\omega) \cong 1 + \frac{4\pi ne^2}{k_BT}\frac{1}{q^2}\,\Psi(u'). \quad \text{(A23)}$$

Here $4\pi ne^2/k_BT = k_D^2$ is the Debye screening constant.

Finally, we obtain

$$\varepsilon(q,\omega) = 1 + \frac{k_D^2}{q^2}\Psi(u') = 1 + \frac{k_D^2}{q^2}\frac{1}{\sqrt{\pi}}\int_{-\infty}^{\infty}\frac{y\, e^{-y^2}}{y-u'-i\delta}dy, \quad \text{(A24)}$$

with $u' = \sqrt{\frac{m_e}{2k_BT}}\frac{\omega}{q}$.

At first sight the integral function here looks different from the Pines expression. However, we can show the identity by making the following change of variables: $y = x/\sqrt{2}$, $u' = \xi/\sqrt{2}$. Then,

$$\frac{1}{\sqrt{\pi}}\int_{-\infty}^{\infty}\frac{y\,e^{-y^2}}{y-u'-i\delta}dy = \frac{1}{\sqrt{2\pi}}\int_{-\infty}^{\infty}\frac{x\,e^{-x^2/2}}{x-\xi-i\delta}dx, \tag{A25}$$

and so

$$\varepsilon(q,\omega) = 1+\frac{k_D^2}{q^2}\,W\left(\frac{\omega}{qv_T}\right) = 1+\frac{k_D^2}{q^2}\,\frac{1}{\sqrt{2\pi}}\int_{-\infty}^{\infty}\frac{x\,e^{-x^2/2}}{x-\xi-i\delta}dx, \tag{A26}$$

with $\xi = \omega/qv_T = \sqrt{\frac{m_e}{k_BT}}\frac{\omega}{q}$, in full agreement with Pines [42].

The real part of ε is the principal value of this expression. Here two alternative expressions may be quoted:

$$W_1(\xi) = 1-\xi^2\int_0^1 \exp\left[\frac{\xi^2}{2}(y^2-1)\right]dy, \tag{A27}$$

or the equivalent formula

$$W_1(\xi) = \frac{1}{2}\int_0^{\infty}\cos\left(\frac{\xi y}{\sqrt{2}}\right)y\,e^{-y^2/4}dy. \tag{A28}$$

Replacing this in Eq. (A26), a direct calculation of $\varepsilon_1(q,\omega)$ can be made.

The imaginary part may also be obtained from Eq. (A19) using the limiting property

$$\frac{1}{x-\xi-i\delta} \to PV\left(\frac{1}{x-\xi}\right)+i\pi\delta(x-\xi), \tag{A29}$$

or taking the limit $\hbar \to 0$ in Eq. (A16). This yields

$$\varepsilon_2(q,\omega) = \frac{m_e\omega_P^2}{2k_BT}\left(\frac{2\pi m_e}{k_BT}\right)^{1/2}\left(\frac{\omega}{q^3}\right)\exp\left[-\frac{m_e}{2k_BT}\left(\frac{\omega}{q}\right)^2\right]. \tag{A30}$$

As is obvious from these expressions all quantum-mechanical terms have disappeared.

The combination of this fully classical solution with the quantum-mechanical approach described in the text is referred to as the semiclassical model (SCLM).

APPENDIX B: APPENDIX B: POLARIZATION AND FLUCTUATION TERMS IN THE ENERGY-LOSS MOMENTS

The formulation given in the text separates the contributions into 0-order and N-order processes. This procedure is fully equivalent to the separation in terms of *polarization* and *fluctuations*, a terminology that is normally used in the standard plasma literature [32,33]. However, we think that the former terminology fits better with the quantum-mechanical framework considered here.

For the sake of comparison with other expression of the stopping power for light particles reported by previous authors [62,63] it is useful to rewrite the expressions developed here as integrals over positive frequencies only. To do this we consider the expressions for the positron stopping power in Eqs. (46) and (47). Changing the integration variable ω by $-\omega$ in Eq. (46) and making use of the relation $N(-\omega) = -[1+N(\omega)]$, we obtain

$$S_{\rm loss} = \frac{2}{\pi}\left(\frac{Ze}{v}\right)^2\int_0^{q_1}\frac{dq}{q}\int_0^{qv-\gamma q^2}\omega[1+N(\omega)] \times {\rm Im}\left[\frac{-1}{\varepsilon(q,\omega)}\right]d\omega. \tag{B1}$$

The term 1 in the square bracket yields the energy loss corresponding to *polarization*, and the term with $N(\omega)$ combines with the "gain" term of Eq. (47) to yield the *fluctuation* term. By rearranging the terms and considering the different integration limits in q and ω, we finally get

$$S = S_{\rm polar} + S_{\rm fluct}, \tag{B2}$$

where

$$S_{\rm polar} = \frac{2}{\pi}\left(\frac{Ze}{v}\right)^2\int_0^{q_1}\frac{dq}{q}\int_0^{qv-\gamma q^2}\omega{\rm Im}\left[\frac{-1}{\varepsilon(q,\omega)}\right]d\omega, \tag{B3}$$

and

$$S_{\rm fluct} = \frac{2}{\pi}\left(\frac{Ze}{v}\right)^2\int_0^{q_1}\frac{dq}{q}\int_{qv-\gamma q^2}^{qv+\gamma q^2}\omega N(\omega){\rm Im}\left[\frac{-1}{\varepsilon(q,\omega)}\right]d\omega + \frac{2}{\pi}\left(\frac{Ze}{v}\right)^2\int_{q_1}^{\infty}\frac{dq}{q}\int_{-qv+\gamma q^2}^{qv+\gamma q^2}\omega N(\omega){\rm Im}\left[\frac{-1}{\varepsilon(q,\omega)}\right]d\omega, \tag{B4}$$

with $q_1 = 2m_pv/\hbar$, $\gamma = \hbar/2m_p$, and m_p is the mass of the test particle.

By comparing with the expressions in Ref. [63] [Eqs. (5) and (6)] we find unexpected differences. On the other hand, our result for the total stopping agrees completely with Eq. (1) of Ref. [62]. We stress here that a careful consideration of the integration limits is required in order to get the correct results.

As a final remark, we must also stress that these expressions are appropriate to describe the stopping of positrons but do not describe the case of electrons since the restrictions imposed by the identity principle are nor included in these formulas, nor in the calculations of the cited references. The relevance of these restrictions can be assessed from the examples given earlier in the text.

A similar analysis can be made for the straggling and inelastic mean-free path. Taking for instance the case of the straggling, we can make the same change of integration variable $\omega \to -\omega$, and considering now the different parity of the integrand we get

$$\Omega^2_{\rm loss} = \frac{2}{\pi}\left(\frac{Ze}{v}\right)^2\hbar\int_0^{q_1}\frac{dq}{q}\int_0^{qv-\gamma q^2}\omega^2[1+N(\omega)] \times {\rm Im}\left[\frac{-1}{\varepsilon(q,\omega)}\right]d\omega, \tag{B5}$$

and following the same procedure as before we obtain

$$\Omega^2 = \Omega^2_{\rm polar} + \Omega^2_{\rm fluct}, \tag{B6}$$

with

$$\Omega^2_{\rm polar} = \frac{2}{\pi}\left(\frac{Ze}{v}\right)^2 \hbar \int_0^{q_1} \frac{dq}{q} \int_0^{qv-\gamma q^2} \omega^2 {\rm Im}\left[\frac{-1}{\varepsilon(q,\omega)}\right] d\omega. \tag{B7}$$

and

$$\Omega^2_{\rm fluct} = \frac{2}{\pi}\left(\frac{Ze}{v}\right)^2 \hbar \int_0^{q_1} \frac{dq}{q} \int_0^{qv-\gamma q^2} \omega^2 2N(\omega) \times {\rm Im}\left[\frac{-1}{\varepsilon(q,\omega)}\right] d\omega + \frac{2}{\pi}\left(\frac{Ze}{v}\right)^2 \hbar \int_0^{q_1} \frac{dq}{q} \int_{qv-\gamma q^2}^{qv+\gamma q^2} \omega^2 N(\omega) \times {\rm Im}\left[\frac{-1}{\varepsilon(q,\omega)}\right] d\omega + \frac{2}{\pi}\left(\frac{Ze}{v}\right)^2 \hbar \int_{q_1}^{\infty} \frac{dq}{q} \int_{-qv+\gamma q^2}^{qv+\gamma q^2} \omega^2 N(\omega) \times {\rm Im}\left[\frac{-1}{\varepsilon(q,\omega)}\right] d\omega. \tag{B8}$$

Notice the different integration limits for q and ω in each of these terms.

Finally, a similar decomposition can be made for the inverse-mean-free path, as the previous one for the straggling, with the only change of omitting the ω^2 factor in the integrals.

[1] T. J. Dolan, *Fusion Research* (Pergamon Press, New York, 2000).

[2] *Fusion Physics*, edited by M. Kikuchi, K. Lackner, and M. Q. Tran (IAEA, Vienna, 2012).

[3] *Atomic and Molecular Processes in Fusion Edge Plasmas*, edited by R. K. Janev (Springer, New York, 1995).

[4] J. Larsen, *Foundations of High-Energy-Density Physics* (Cambridge University Press, Cambridge, 2017).

[5] A. O. Benz, *Plasma Astrophysics* (Kugler, New York, 2002).

[6] B. M. Smirnov, *Plasma Processes and Plasma Kinetics* (Wiley, Weinheim, 2007).

[7] P. M. Platzman and P. A. Wolff, *Elementary Excitations in Solid-State Plasmas* (Academic Press, New York, 1973).

[8] C. D. Archubi and N. R. Arista, Unified description of interactions and energy loss of particles in dense matter and plasmas, Phys. Rev. A **102**, 052811 (2020).

[9] J. Neufeld and R. H. Ritchie, Passage of charged particles through plasma, Phys. Rev. **98**, 1632 (1955).

[10] T. Kihara and O. Aono, Unified theory of relaxations in plasmas, J. Phys. Soc. Jpn. **18**, 837 (1963).

[11] N. R. Arista and W. Brandt, Energy loss and straggling of charged particles in plasmas of all degeneracies Phys. Rev. A **23**, 1898 (1981).

[12] G. Maynard and C. Deutsch, Energy loss and straggling of ions with any velocity in dense plasmas at any temperature, Phys. Rev. A **26**, 665 (1982).

[13] L de Ferrariis and N. R. Arista, Classical and quantum mechanical treatments of the energy loss of charged particles in dilute plasmas, Phys. Rev. A **29**, 2145 (1984).

[14] N. R. Arista, Low-velocity stopping power of semi-degenerate quantum plasmas, J. Phys. C: Solid State Phys. **18**, 5127 (1985).

[15] T. Peter and J. Meyer-ter-Vehn, Energy loss of heavy ions in dense plasma. Linear and nonlinear Vlasov theory for the stopping power, Phys. Rev. A **43**, 1998 (1991).

[16] A. Bret and C. Deutsch, Straggling of an extended charge distribution in a partially degenerate plasma, Phys. Rev. E **48**, 2989 (1993).

[17] E. M. Bringa and N. R. Arista, Energy loss of correlated ions in plasmas: Collective and individual contributions, Phys. Rev. E **54**, 4101 (1996).

[18] G.-Q. Wang, Y.-N. Wang, and Z. L. Miskovic, Coulomb explosion and energy loss of fast C_{60} clusters in plasmas, Phys. Plasmas **12**, 042702 (2005).

[19] Z. L. Miskovic, Y.-N Wang, and Y.-H. Song, Dynamics of fast molecular ions in solid and plasmas: A review of recent theoretical developments, Nucl. Instrum. Methods Phys. Res., Sect. B **256**, 57 (2007).

[20] M. D. Barriga-Carrasco, Effect of target electron collisions on energy loss straggling in plasmas of all degeneracies, Nucl. Instrum. Methods Phys. Res. Sect. A **577**, 371 (2007).

[21] M. D. Barriga-Carrasco, Heavy ions charge-state distribution effects on energy loss in plasmas, Phys. Rev. E **88**, 043107 (2013).

[22] C. F. Clauser and N. R. Arista, Stopping power of dense plasmas, Phys. Rev. E **97**, 023202 (2018).

[23] L. González-Gallego, M. D. Barriga-Carrasco, and J. Vázquez-Moyano, Reduced stopping power of protons propagation through hot plasmas, Phys. Plasmas **28**, 043103 (2021).

[24] L. R. Grisham *et al.*, Neutral beam injection on the tokamak fusion test reactor, Nucl. Instrum. Methods Phys. Res., Sect. B **24-25**, 741 (1987).

[25] J. D. Strahan *et al.*, Fusion Production From TFTR Plasmas Fueled with Deuterium and Tritium, Phys. Rev. Lett. **72**, 3526 (1994).

[26] R. J. Hawryluk *et al.*, Confinement and Heating of Deuterium-Tritium Plasmas, Phys. Rev. Lett. **72**, 3530 (1994).

[27] T. L. Mehlhorn, A finite material temperature model for ion energy deposition in ion-driven inertial confinement fusion targets, J. Appl. Phys. **52**, 6522 (1981).

[28] K. A. Long and N. A. Tahir, Theory and calculation of the energy loss of charged particles in inertial confinement fusion burning plasmas, Nucl. Fusion **26**, 555 (1986).

[29] R. C. Arnold and J. Meyer-ter-Vehn, Inertial confinement fusion driven by heavy-ion beams, Rep. Prog. Physics **50**, 559 (1987).

[30] Y. I. Kolesnichenko, The role of alpha particles in tokamak reactors, Nucl. Fusion **20**, 727 (1980).

[31] S. Putvinsky *et al.*, Alpha-particle physics in tokamaks, Philos. Trans. R. Soc. A **357**, 493 (1999).

[32] A. G. Sitenko, *Electromagnetic Fluctuations in Plasma* (Academic Press, New York, 1967).

[33] A. I. Akhiezer, I. A. Akhiezer, R. V. Polovin, A. G. Sitenko, and K. N. Stepanov, *Plasma Electrodynamics, Non-Linear Theory and Fluctuations* (Pergamon Press, New York, 1975), Vol. 2.

[34] H. A. Bethe and J. Ashkin, in *Passage of Radiation Through Matter*, edited by E. Segré, Experimental Nuclear Physics (Wiley, New York, 1953).

[35] L. D. Landau and E. M. Lifshitz, *Quantum Mechanics: Non-Relativistic Theory* (Pergamon Press, New York, 1977).

[36] V. I. Ochkur, Soviet Phys. JETP **47**, 1766 (1964).

[37] B. H. Bransden, *Atomic Collision Theory* (W. A. Benjamin, New York, 1970).

[38] J. M. Fernández-Varea, R. Mayol, D. Liljequist, and F. Salvat, J. Phys.: Condens. Matter **5**, 3593 (1993).

[39] R. García-Molina, I. Abril, I. Kyriakou, and D. Emfietzoglou, Inelastic scattering and energy loss of swift electron beams in biologically relevant materials, Surf. Interface Anal. **49**, 11 (2017).

[40] P. de Vera and R. García-Molina, Electron inelastic mean free paths in condensed matter down to a few electronvolts, J. Phys. Chem. C **123**, 2075 (2019).

[41] C. D. Archubi and N. R. Arista, A comparative study of threshold effects in the energy loss moments of protons, electrons and positrons using dielectric models for band gap materials, Eur. Phys. J. B **90**, 18 (2017).

[42] D. Pines, Classical and quantum plasmas, Plasma Phys. **2**, 5 (1961), Note: a minus sign is missing in the exponential term $\exp(x^2/2)$ in Eq. (3.16) of this reference.

[43] S. Ichimaru, *Basic Principles of Plasma Physics* (CRC Press, 1973).

[44] N. A. Krall and A. W. Trivelpiece, *Principles of Plasma Physics* (McGraw-Hill, New York, 1973).

[45] C. Gouedard and C. Deutsch, Dense electron-gas response at any degeneracy, J. Math. Phys. **19**, 32 (1978).

[46] N. R. Arista and W. Brandt, Dielectric response of quantum plasmas in thermal equilibrium, Phys. Rev. A **29**, 1471 (1984).

[47] C. D. Archubi and N. R. Arista, Extended wave-packet model to calculate energy-loss moments of protons in matter, Phys. Rev. A **96**, 062701 (2017).

[48] T. Kaneko, Wave packet theory of bond electrons, Phys. Rev. A **40**, 2188 (1989).

[49] T. Kaneko, Partial and total electronic stoppings of solids and atoms for energetic ions, Phys. Status Solidi B **156**, 49 (1989).

[50] T. Kaneko, Partial and total electronic stopping cross sections of atoms and solids for protons, At. Data Nucl. Data Tables **53**, 271 (1993).

[51] J. Lindhard, On the properties of a gas of charged particles, Mat. Fys. Medd. Dan. Vid. Selsk **28**, 1 (1954).

[52] R. H. Ritchie, Interaction of charged particles with a degenerate Fermi-Dirac electron gas, Phys. Rev. **114**, 644 (1959).

[53] D. Pines, *Elementary Excitations in Solids* (W. A. Benjamin, New York, 1964).

[54] W. Brandt and J. Reinheimer, Theory of semiconductor response to charged particles, Phys. Rev. B **2**, 3104 (1970).

[55] J. Valdes, P. Vargas, and N. Arista, Differences in the energy loss of protons and positive muons in solids, Nucl. Instrum. Methods Phys. Res. Sect. B **174**, 1 (2001).

[56] P. Sigmund, *Particle Penetration and Radiation Effects* (Springer, Berlin, 2006).

[57] A. Mann and W. Brandt, Material dependence of low velocity stopping power, Phys. Rev. B **24**, 4999 (1981).

[58] F. Perrot, Temperature-dependent nonlinear screening of a proton in an electron gas, Phys. Rev. A **25**, 489 (1982).

[59] I. Nagy, A. Arnau, P. M. Echenique, and K. Ladányi, Stopping power of a finite-temperature electron gas for slow unit charges, Phys. Rev. A **43**, 6038 (1991).

[60] C. E. Celedón, G. H. Lantschner, and N. R. Arista, Experimental determinations and computer simulations of the energy loss straggling of slow ions in thin foils, Nucl. Instrum. Meth. Phys. Res. B **315**, 21 (2013).

[61] B. D. Fried and S. D. Conte, *The Plasma Dispersion Function* (Academic Press, New York, 1961).

[62] W. D. Kraeft and B. Strege, Energy loss of charged particles moving in a plasma, Phys. A (Amsterdam, Neth.) **149A**, 313 (1988).

[63] B. Strege and W. D. Kraeft, Stopping power of charged particles in a plasma, Laser Part. Beams **10**, 227 (1992).